

# M2-brane indices on Higgs vacua

---

Chiung Hwang, Chang Lei, and Yuezhang Tang

*Interdisciplinary Center for Theoretical Study, University of Science and Technology of China,  
Hefei, Anhui 230026, China*

*Peng Huanwu Center for Fundamental Theory,  
Hefei, Anhui 230026, China*

*E-mail:* [chiung@ustc.edu.cn](mailto:chiung@ustc.edu.cn), [leich@mail.ustc.edu.cn](mailto:leich@mail.ustc.edu.cn),  
[yuezhangtang@ustc.edu.cn](mailto:yuezhangtang@ustc.edu.cn)

**ABSTRACT:** As an exact count of protected states, the superconformal index provides a powerful probe into holography and quantum aspects of gravity, reproducing the Bekenstein–Hawking entropy of supersymmetric AdS black holes in the large- $N$  limit. As a step toward understanding quantum black hole microstates, we study the finite- $N$  index of the 3d ADHM quiver gauge theory, a UV description of the 3d  $\mathcal{N} = 8$  SCFT dual to M-theory on  $\text{AdS}_4 \times S^7$ . In this note, we analyze both microcanonical and canonical features of the superconformal index. By computing the index to sufficiently high orders, we identify signatures of quantum black hole states in the finite- $N$  spectrum of the ADHM quiver, which align with the leading large- $N$  contribution reflecting the holographic dual black hole entropy. Furthermore, we introduce the complex- $\beta$  phase diagram of the index, which exhibits distinct peaks potentially associated with different gravitational saddles. To enable high-order computations, we employ the factorized index and also examine its Higgs branch Hilbert series limit. Our results demonstrate that the finite- $N$  index encodes rich information about black hole microstates and their quantum gravitational interpretation.

---

## Contents

<b>1</b>	<b>Introduction</b>	<b>1</b>
<b>2</b>	<b>Superconformal indices of M2-branes at finite <math>N</math> and complex-<math>\beta</math> phase diagrams</b>	<b>3</b>
2.1	$N = 1$	8
2.2	$N = 2, 3$	9
2.2.1	Complex- $\beta$ phase diagram	13
2.3	$N = 4, 5$	17
<b>3</b>	<b>BPS indices on Higgs vacua of the 3d ADHM with a single flavor</b>	<b>19</b>
<b>4</b>	<b>Factorization of the 3d ADHM index with multiple flavors</b>	<b>24</b>
4.1	Examples	27
4.2	Limit to the Higgs branch Hilbert series	28
<b>5</b>	<b>Discussion</b>	<b>32</b>
<b>A</b>	<b>Numerical index data</b>	<b>34</b>
A.1	$F = 1$	34
A.2	$F = 2$	39

---

## 1 Introduction

The superconformal index [1–3] has become a powerful tool in the study of holography, providing an exact count of protected states in strongly coupled superconformal theories (SCFTs) and offering a unique window into quantum aspects of their gravitational duals. Remarkably, in many holographic examples, the superconformal index reproduces the Bekenstein–Hawking entropy of supersymmetric AdS black holes in the large- $N$  limit,<sup>1</sup> establishing a direct bridge between field-theoretic state counting and semiclassical gravity. While much of the recent progress has focused on 4d  $\mathcal{N} = 4$  super Yang–Mills (SYM) theory, the 3d  $\mathcal{N} = 8$  SCFT, which is holographically dual to M-theory on  $\text{AdS}_4 \times S^7$ , provides an equally rich setting to explore these ideas.

However, while the large- $N$  limit reveals the thermodynamic behavior of black holes, it conceals the detailed structure of individual microstates. This limitation has motivated growing interest in studying theories at finite  $N$ , where one can hope to resolve the microstate spectrum directly from the field theory. For example, in the case of 4d  $\mathcal{N} = 4$  SYM

---

<sup>1</sup>See, for instance, [4–8] for early results in each spacetime dimension. Also see a review [9] for more examples including other types of supersymmetric indices, including the pioneering work on the topologically twisted index [10].

theory, it was found that even at small  $N$ , the growth of the (signed) BPS state degeneracies computed from the index closely approximates the black hole entropy inferred from the large- $N$  analysis [11, 12]. This suggests that a meaningful notion of black hole microstates persists at finite  $N$ , and tools such as supercharge cohomology have been employed to identify and construct black hole-like states explicitly at finite  $N$  [13–19].

These developments provide compelling evidence that the finite- $N$  index can serve as a refined probe of quantum gravity. In this note, we therefore aim to examine both the microcanonical and canonical aspects of the *finite- $N$*  superconformal index for the 3d ADHM quiver gauge theory, one of the UV gauge descriptions of the 3d  $\mathcal{N} = 8$  SCFT. Our study follows two complementary approaches. First, we compare the signed degeneracies obtained from the finite- $N$  indices for the ADHM quiver with the large- $N$  entropy derived in [8]. Despite the small values of  $N$ , we observe remarkably good agreement between these quantities. Second, regarding it as a canonical partition function, we explore the possible phases of the superconformal index by varying a chemical potential over the complex plane. For standard thermal partition functions, the imaginary part of the chemical potential typically reflects the non-unitarity, such as decay rates or non-conserved particle numbers in open systems. In contrast, for the index, the imaginary part of the chemical potential plays a slightly different role: it interferes with the cancellations between bosonic and fermionic contributions due to their relative sign in the definition of the index. In this sense, the complex chemical potential controls which contributions are amplified or suppressed in the index.

More precisely, for the contribution arising from a conjugate pair of complex saddles, labeled by  $a$ , their microcanonical signs for given charges, collectively denoted as  $Q$ , are determined by the imaginary part of the complexified entropy  $S_a$  as follows:

$$I_a(Q) = e^{S_a(Q)} + e^{S_a^*(Q)} \sim e^{\text{Re } S_a(Q)} \cos(\text{Im } S_a(Q)), \quad (1.1)$$

where the overall sign is governed by the cosine factor involving  $\text{Im } S_a(Q)$ . The index in the canonical ensemble is then given by

$$\mathcal{I}(\beta) = \sum_a \sum_Q I_a(Q) e^{-\beta Q}, \quad (1.2)$$

and the contribution of saddle  $a$  is maximized when

$$\pm \frac{\Delta \text{Im } S_a(Q)}{\Delta Q} - \text{Im } \beta = 2\pi k, \quad k \in \mathbb{Z}, \quad (1.3)$$

which determines the location of the peak associated with saddle  $a$  in the complex- $\beta$  phase diagram of the index. This analysis suggests that different saddles, regardless of whether dominant or not, can be distinguished by examining the complex- $\beta$  phase diagram.

For this purpose, however, we require a computational tool capable of evaluating the index to sufficiently high orders, which is challenging using the standard matrix integral formula derived from supersymmetric localization [20, 21]. To overcome this difficulty, we employ the so-called factorized index derived in [8], which proves to be more efficient than the matrix integral formula for numerical computations for the index. Moreover, this

formula naturally decomposes the index into contributions from discrete Higgs vacua of the theory with generic real masses. These vacua can also be related to solutions of the Bethe ansatz equations (BAEs) associated with 3d supersymmetric partition functions, reflecting the universality of the factorization structure for partition functions on manifolds that are  $S^1$  fibered over  $S^2$  [22–30]. This connection to BAE solutions may, in turn, suggest a gravitational interpretation of the saddles encoded in the complex- $\beta$  phase diagram.

This formula has been derived only in the single-flavor case. In this work, we extend the derivation and present a general formula for the ADHM theory with multiple flavors, dual to M-theory on  $\text{AdS}_4 \times S^7/\mathbb{Z}_F$ , where  $F$  denotes the number of flavors. We further explore a particular limit of the factorized index that yields the refined Higgs branch Hilbert series [31], offering insight into the types of states contributing to each Higgs vacuum.

The rest of this note is organized as follows. In Section 2, we evaluate the superconformal index of the ADHM quiver with a single flavor for various gauge ranks  $N$ , using the factorization formula. Based on this numerical data, we analyze the complex- $\beta$  phase diagrams for  $N = 2$  and  $N = 3$ , which display expected peaks associated with standard graviton and black hole states. Interestingly, the  $N = 3$  case also exhibits an additional peak, suggesting the contribution of an extra quantum gravitational saddle. In Section 3, we analyze the index for each Higgs vacuum and find that the additional peak is associated with the Higgs vacua corresponding to linear Young diagrams, where only one of the two scalars  $Y$  and  $Z$  in the adjoint hypermultiplet acquires a vacuum expectation value. In Section 4, we extend the previous derivation of the factorized index for the single-flavor case to theories with multiple flavors. The Higgs branch Hilbert series limit is also discussed. Finally, in Section 5, we conclude with remarks and discuss limitations. The explicit index data is provided in appendix A.

## 2 Superconformal indices of M2-branes at finite $N$ and complex- $\beta$ phase diagrams

The low-energy dynamics of M2-branes probing  $\mathbb{C}^4$  can be described by the three-dimensional  $\mathcal{N} = 8$  SCFT, which allows several dual gauge descriptions. A notable pair, related by the 3d  $SL(2, \mathbb{Z})$  duality, would be the  $U(N) \times U(N)$  ABJM theory with the Chern-Simons level  $k = 1$  [32] and the  $\mathcal{N} = 4$  supersymmetric Yang-Mills theory with one fundamental and one adjoint hypermultiplets, dubbed the ADHM quiver theory (with a single flavor in this case).<sup>2</sup> While only part of the  $\mathcal{N} = 8$  supersymmetry is manifest in both descriptions,  $\mathcal{N} = 6$  and  $\mathcal{N} = 4$ , respectively, it is enhanced to  $\mathcal{N} = 8$  at the IR fixed point. Similarly to 4d  $\mathcal{N} = 4$  SYM, these theories are of great interest in the context of the AdS/CFT correspondence because the 3d  $\mathcal{N} = 8$  SCFT is holographically dual to M-theory on  $\text{AdS}_4 \times S^7$ . In particular, the large- $N$  limit of their supersymmetric indices have been discussed in

---

<sup>2</sup>The name “ADHM” comes from the fact that the Higgs branch of this theory coincides with the instanton moduli space constructed by the ADHM method [33].

great detail and shown to capture the Bekenstein–Hawking entropy of dual black holes [8, 10, 29, 34, 35].<sup>3</sup>

Although large- $N$  analysis certainly helps us understand the statistical aspect of black hole entropy in a holographic framework, it unfortunately reveals little about the individual microstates of the black hole. For this reason, there has been another line of discussion on this issue, approached from the opposite direction: instead of taking the large- $N$  limit, one attempts to understand dual gravity states, including those of black holes, by analyzing the spectrum of a field theory at fixed  $N$ . Firstly, it was observed that for 4d  $\mathcal{N} = 4$  SYM theory, even with very small values of  $N$ , the enumeration of the number of states using the superconformal index fits surprisingly well with the growth of the number of states expected in the large- $N$  limit [11, 12]. Since this large- $N$  result reproduces the Bekenstein–Hawking entropy of the dual black hole [4–6, 37, 38], it is natural to anticipate that there should be a notion of black hole states even for small  $N$ . Indeed, it was proposed that the graviton states and the black hole states can be distinguished at finite values of  $N$  by examining how the exactness of a state under a chosen supercharge changes when  $N$  varies [13], and some examples of black hole states have been explicitly constructed within the supercharge cohomology [14–19]. Furthermore, it was also shown that the superconformal index captures other types of gravity solutions, e.g., grey galaxies [39, 40].

Hence, we expect that the superconformal index at finite  $N$  contains rich information about the gravity states, which should work not only for 4d  $\mathcal{N} = 4$  SYM but also for general holographic field theories, such as the 3d  $\mathcal{N} = 8$  SCFT mentioned earlier. However, compared to the 4d case, even the simple enumeration of the number of states is more cumbersome in 3d due to the contributions from the non-perturbative monopole states, which give rise to infinite summations in the standard matrix integral formula for the index that can be obtained from supersymmetric localization [20, 21].

In this section, we aim to circumvent this issue by simplifying the computation by means of the so-called factorization method for the 3d superconformal index [24, 41, 42]. As we will show shortly, using the factorized index, we are able to compute the (unrefined) index of the 3d ADHM quiver theory up to reasonably high charges to compare with the analytic result from the large- $N$  analysis.

Let us briefly review factorization of the superconformal index of the ADHM theory. Generally, the superconformal index of a 3d  $\mathcal{N} = 2$  supersymmetric gauge theory can be defined as a supersymmetric partition function on  $S^2 \times S^1$  with periodic boundary condition along  $S^1$  [3]:

$$\mathcal{I} = \text{Tr}(-1)^F e^{-\beta' \{Q, S\}} e^{-\beta(E+j)} e^{-\sum_i \Delta_i Q_i} \quad (2.1)$$

where  $E$  is the energy, and  $j$  is the angular momentum on  $S^2$ . Each  $Q_i$  is a global symmetry charge commuting with chosen supercharges  $Q$  and  $S = Q^\dagger$  satisfying

$$\{Q, S\} = E - R - j \geq 0 \quad (2.2)$$

---

<sup>3</sup>See [36] for a different supersymmetric background. See also [9] for a comprehensive review.

	$U(N)_G$	$U(1)_w$	$U(1)_z$	$U(1)_t$	$U(1)_R$
$\Phi$	$\mathbf{N}$	0	0	1/2	1/2
$\tilde{\Phi}$	$\bar{\mathbf{N}}$	0	0	1/2	1/2
$X$	adj	0	0	-1	1
$Y$	adj	0	1	1/2	1/2
$Z$	adj	0	-1	1/2	1/2
$V^\pm$	$\mathbf{1}$	$\pm 1$	0	-1/2	1/2

**Table 1.** The symmetries of the ADHM quiver gauge theory with a single flavor and the charges of the matter fields (in the  $\mathcal{N} = 2$  notation) and, as examples, the monopole operators of the minimal flux,  $V^\pm$ .

where  $R$  is the  $U(1)_R$  charge. As usual, only the BPS states annihilated by  $Q$  and  $S$ , which thus satisfy

$$E = R + j, \quad (2.3)$$

contribute to the index, and the index is independent of  $\beta'$ . Using the supersymmetric localization on the Coulomb branch, one can derive the matrix integral formula [20, 21], which, for the ADHM quiver with a single flavor, is given by

$$\begin{aligned} \mathcal{I}(w, z, t, q) = & \frac{1}{N!} \sum_{m \in \mathbb{Z}^N / S_N} \oint \left( \prod_{a=1}^N \frac{ds_a}{2\pi i s_a} w^{m_a} t^{-|m_a|/2} q^{|m_a|/2} \right) \times \\ & \left( \prod_{1 \leq a \neq b \leq N} (1 - s_a s_b^{-1} q^{|m_a - m_b|}) \right) \left( \prod_{a=1}^N \frac{(s_a^{-1} t^{-\frac{1}{2}} q^{\frac{3}{2} + |m_a|}; q^2)}{(s_a t^{\frac{1}{2}} q^{\frac{1}{2} + |m_a|}; q^2)} \frac{(s_a t^{-\frac{1}{2}} q^{\frac{3}{2} + |m_a|}; q^2)}{(s_a^{-1} t^{\frac{1}{2}} q^{\frac{1}{2} + |m_a|}; q^2)} \right) \times \\ & \left( \prod_{a,b=1}^N \frac{(s_a^{-1} s_b t q^{1+|-m_a+m_b|}; q^2) (s_a^{-1} s_b z^{-1} t^{-\frac{1}{2}} q^{\frac{3}{2}+|-m_a+m_b|}; q^2) (s_a^{-1} s_b z t^{-\frac{1}{2}} q^{\frac{3}{2}+|-m_a+m_b|}; q^2)}{(s_a s_b^{-1} t^{-1} q^{1+|m_a-m_b|}; q^2) (s_a s_b^{-1} z t^{\frac{1}{2}} q^{\frac{1}{2}+|m_a-m_b|}; q^2) (s_a s_b^{-1} z^{-1} t^{\frac{1}{2}} q^{\frac{1}{2}+|m_a-m_b|}; q^2)} \right), \end{aligned} \quad (2.4)$$

where we have used the shorthand  $(a; q^2)$  for the infinite q-Pochhammer symbol,  $(a; q^2)_\infty = \prod_{k=0}^\infty (1 - a q^{2k})$ .  $w$  ( $= e^{-\Delta_w}$ ),  $z$  ( $= e^{-\Delta_z}$ ), and  $t$  ( $= e^{-\Delta_t}$ ) are fugacities for the global symmetries of the ADHM theory with a single flavor, shown in Table 1 with the corresponding fugacities indicated in their subscript, except the R-symmetry  $U(1)_R$ , whose fugacity, up to a shift by angular momentum, is  $q = e^{-\beta}$ . These symmetries are actually combined and enhanced to the  $Spin(8)_R$  symmetry in the IR. As explained, the localization formula for the 3d index includes the infinite summation over quantized magnetic flux on  $S^2$ .

Using this formula, the large- $N$  behavior of the index has been examined. The leading contribution to the BPS free energy, which is defined as the negative logarithm of the index,

is given by [8]

$$\mathcal{F} = -\log \mathcal{I} \approx \pm i \frac{4\sqrt{2}N^{\frac{3}{2}}}{3} \frac{\sqrt{\Delta_1\Delta_2\Delta_3\Delta_4}}{2\beta}, \quad (2.5)$$

$$\sum_{i=1}^4 \Delta_i = \pm 2\pi i + 2\beta, \quad (2.6)$$

where  $\Delta_i$ 's are combinations of  $\Delta_{w,z,t}$  and  $\beta$ , which we do not display here since eventually we are interested in the unrefined limit where  $\Delta_w = \Delta_z = \Delta_t = 0$ . One condition imposed on them is the real part of  $\sqrt{\Delta_1\Delta_2\Delta_3\Delta_4}$  is taken to be positive. See [8] for further details.

In addition to this matrix integral formula, there is another useful expression for the index obtained by the factorization method [24, 41, 42]. This method rearranges the residues of the integral together with the flux summation, resulting in the factorized form of the index into the vortex and anti-vortex partition functions on  $\mathbb{R}^2 \times S^1$ , which is naturally anticipated from the Higgs branch localization [26, 27] as well as the holomorphic block [22, 23].

More precisely, the factorized index is written as the summation of the product of the perturbative part and the vortex and anti-vortex parts over discrete Higgs vacua of the theory with generic real masses for global symmetries [8]:<sup>4</sup>

$$\mathcal{I}(w, z, t, q) = \sum_{|\mathcal{Y}|=N} Z_{\text{pert}}^{\mathcal{Y}}(z, t, q) Z_{\text{vort}}^{\mathcal{Y}}(w, z, t, q) Z_{\text{vort}}^{\mathcal{Y}}(w^{-1}, z^{-1}, t^{-1}, q^{-1}) \quad (2.7)$$

with

$$\begin{aligned} Z_{\text{pert}}^{\mathcal{Y}}(z, t, q) &= \left( \prod_{\mathbf{a} \neq \mathbf{b} \in \mathcal{Y}} (1 - v_{\mathbf{a}}^{-1} v_{\mathbf{b}}) \right) \left( \prod_{\mathbf{a} \in \mathcal{Y}} \frac{(v_{\mathbf{a}} q^2; q^2)}{(v_{\mathbf{a}}^{-1}; q^2)} \frac{(v_{\mathbf{a}}^{-1} (tq)^{-1} q^2; q^2)}{(v_{\mathbf{a}} tq; q^2)} \right) \\ &\times \left( \prod_{\mathbf{a}, \mathbf{b} \in \mathcal{Y}} \frac{(v_{\mathbf{a}} v_{\mathbf{b}}^{-1} tq; q^2) (v_{\mathbf{a}} v_{\mathbf{b}}^{-1} (zt^{\frac{1}{2}} q^{\frac{1}{2}})^{-1} q^2; q^2) (v_{\mathbf{a}} v_{\mathbf{b}}^{-1} (z^{-1} t^{\frac{1}{2}} q^{\frac{1}{2}})^{-1} q^2; q^2)}{(v_{\mathbf{a}}^{-1} v_{\mathbf{b}} (tq)^{-1} q^2; q^2) (v_{\mathbf{a}}^{-1} v_{\mathbf{b}} zt^{\frac{1}{2}} q^{\frac{1}{2}}; q^2) (v_{\mathbf{a}}^{-1} v_{\mathbf{b}} z^{-1} t^{\frac{1}{2}} q^{\frac{1}{2}}; q^2)} \right), \end{aligned} \quad (2.8)$$

$$\begin{aligned} Z_{\text{vort}}^{\mathcal{Y}}(w, z, t, q) &= \sum_{k_{\mathbf{a}}} \left( wt^{\frac{1}{2}} q^{-\frac{1}{2}} \right)^{\sum_{\mathbf{a} \in \mathcal{Y}} k_{\mathbf{a}}} \left( \prod_{\mathbf{a} \in \mathcal{Y}} \frac{(v_{\mathbf{a}}^{-1}; q^2)_{-k_{\mathbf{a}}}}{(v_{\mathbf{a}}^{-1} t^{-1} q; q^2)_{-k_{\mathbf{a}}}} \right) \\ &\times \left( \prod_{\mathbf{a} \neq \mathbf{b} \in \mathcal{Y}} \frac{(v_{\mathbf{a}}^{-1} v_{\mathbf{b}} zt^{\frac{1}{2}} q^{\frac{1}{2}}; q^2)_{-k_{\mathbf{a}}+k_{\mathbf{b}}}}{(v_{\mathbf{a}}^{-1} v_{\mathbf{b}}; q^2)_{-k_{\mathbf{a}}+k_{\mathbf{b}}}} \frac{(v_{\mathbf{a}}^{-1} v_{\mathbf{b}} t^{-1} q; q^2)_{-k_{\mathbf{a}}+k_{\mathbf{b}}}}{(v_{\mathbf{a}}^{-1} v_{\mathbf{b}} zt^{-\frac{1}{2}} q^{\frac{3}{2}}; q^2)_{-k_{\mathbf{a}}+k_{\mathbf{b}}}} \right) \end{aligned} \quad (2.9)$$

where the vanishing factors appearing in the expression must be discarded. The  $U(N)$  ADHM with a single flavor with generic real masses has discrete Higgs vacua that can be

---

<sup>4</sup>The perturbative part  $Z_{\text{pert}}^{\mathcal{Y}}$  can also be factorized, where each piece can be interpreted as the contribution of perturbative excitations on  $\mathbb{R}^2 \times S^1$  with appropriate boundary conditions.

labeled by Young diagrams of size  $N$ , which are denoted by  $\mathcal{Y}$  in (2.7).  $v_{\mathbf{a}}$  for  $\mathbf{a} \in \mathcal{Y}$  is given by

$$v_{\mathbf{a}} = z^{i(\mathbf{a})-j(\mathbf{a})} (tq)^{\frac{1}{2}(i(\mathbf{a})+j(\mathbf{a})-2)} \quad (2.10)$$

where  $(i(\mathbf{a}), j(\mathbf{a}))$  is the position of box  $\mathbf{a}$  in the Young diagram  $\mathcal{Y}$ .  $k_{\mathbf{a}}$  is a non-negative integer assigned to each  $\mathbf{a}$  such that these integers are non-decreasing along each row and column of  $\mathcal{Y}$ , starting from the initial box at position  $(1, 1)$ . Importantly, it turns out this expression is much more efficient than the matrix integral formula (2.4) in numerically calculating the index. Hence, we attempt to evaluate the indices of M2-branes using this expression, for some finite values of  $N$ , and compare them with the results from the large- $N$  analysis, capturing the Bekenstein–Hawking black hole entropy [8, 43].

Despite the fact that the general index includes refined charge information, for computational simplicity, we focus only on the overall scaling of the number of states. Thus, as mentioned, we simplify the index by taking  $t, z, w \rightarrow 1$ . The resulting index is

$$\mathcal{I}(\beta) = \text{Tr}(-1)^F q^{E+j} = \text{Tr}(-1)^F x^Q = \sum_{Q=0}^{\infty} I(Q) x^Q \quad (2.11)$$

where  $x \equiv q^{\frac{1}{2}} = e^{-\beta/2}$  and  $Q \equiv 2E + 2j$ . Remember the global symmetries of the ADHM theory with a single flavor are enhanced to the  $Spin(8)_R$  symmetry in the IR, whose Cartan charges, conjugate to  $\Delta_i$ , relate to the  $U(1)_R$  charge as follows:

$$R = \frac{1}{2} (Q_1 + Q_2 + Q_3 + Q_4), \quad (2.12)$$

where  $Q_i$ 's are integer-quantized. Roughly speaking, the  $Q_i$  count the excitations of the adjoint fields  $Y$  and  $Z$ , as well as those of the monopole operators with positive and negative fluxes, respectively. Thus, the single charge  $Q$  acting on the BPS states satisfies

$$Q = 2E + 2j = 2R + 4j = Q_1 + Q_2 + Q_3 + Q_4 + 4j. \quad (2.13)$$

Note that the expression (2.7) is singular in the unrefined limit, which is anticipated because the real part of  $\Delta_i$  is associated with the real mass, and the theory has the continuous vacuum moduli space rather than discrete Higgs vacua if the real masses are turned off. It means there should be zero modes whose contribution to the vortex partition function on  $\mathbb{R}^2 \times S^1$  diverges in the unrefined limit. Nevertheless, after the summation over the Higgs vacua, the final superconformal index does not have such a singularity, and one can safely take the unrefined limit. We will revisit this point in Section 3.

Accordingly, the leading part of the large- $N$  free energy (2.5) is simplified to

$$\mathcal{F}|_{\text{leading}} = -\log \mathcal{I}|_{\text{leading}} = -i \frac{4\sqrt{2}N^{\frac{3}{2}}}{3} \frac{\Delta^2}{2\beta}, \quad \Delta = \frac{2\pi i + 2\beta}{4} \quad (2.14)$$

where we have assumed  $\sqrt{\Delta^4} = -\Delta^2$  because the real part of  $\Delta^2$  at the extremum will turn out to be negative. From now on, for simplicity, we will use  $\mathcal{F}$  to denote only the



leading part. By taking the Legendre transformation with respect to  $\beta$ , which is conjugate to  $E + j = Q/2$ , we obtain (the negative of) the large- $N$  entropy  $S$  as follows:

$$S(Q; N^{\frac{3}{2}}) = \frac{\sqrt{2}\pi N^{\frac{3}{2}}}{3} \left( \sqrt{1 - \frac{3}{\sqrt{2}} \frac{iQ}{N^{\frac{3}{2}}}} - 1 \right), \quad (2.15)$$

$$\beta = -\frac{i\pi}{\sqrt{1 - \frac{3}{\sqrt{2}} \frac{iQ}{N^{\frac{3}{2}}}}}, \quad (2.16)$$

where we have chosen the solution ensuring both  $\text{Re } \beta > 0$  and  $\text{Re } S > 0$  as required for the macroscopic entropy. Its exponential should approximate the coefficient of the index for a given  $Q$  in the large- $N$  limit.

## 2.1 $N = 1$

Let us start with  $N = 1$ . The  $N = 1$  case is rather special because in this case the theory is free and dual to a pair of a hyper and a twisted hypermultiplets. This relation can be understood as both mirror symmetry [44] and Aharony duality [45].<sup>5</sup> The equality of their indices has been analytically proved in a few different ways, e.g., using the q-binomial theorem [49] and using the wall-crossing of the vortex quantum mechanics index [50].

The crucial point is that these decoupled hypers persist even in the higher  $N$  cases, implying that there is no black hole state in the  $N = 1$  case. According to recent discussions, at finite  $N$ , one can distinguish the graviton states and the black hole states, or more precisely, the states corresponding to smooth horizonless geometries and the others, by their supercharge cohomology [13]. It has been proposed that the smooth horizonless states remain BPS for arbitrary  $N$ , which is why they are called monotone states, while the black hole states are accidentally BPS for some range of  $N$ , which is why they are called fortuitous states, instead. Since the states in the  $N = 1$  case remain decoupled and BPS for arbitrary  $N$ , all of them are monotone and thus correspond to smooth horizonless states.

Since  $N = 1$ , all the corrections in the large- $N$  expansion are of the same order as the leading contribution. Thus, there is no reason to expect that the actual  $N = 1$  index and that from the leading large- $N$  free energy (2.14) would agree. Furthermore, the fact that the  $N = 1$  case does not include any black hole state makes the agreement more unlikely because, in the large- $N$  limit, this leading piece is interpreted as the black hole contribution. However, rather unexpectedly, in the actual comparison, this leading contribution provides a reasonably good approximation of the index, at least in the certain range of  $Q$ . See the left plot in Figure 1. For comparison, we also present the graviton index (red dots) derived from the gravity side, which is given by [3]

$$\mathcal{I}_{N=\infty}^{\text{graviton}}(x) = \text{PE}[g(x)] = \exp \left[ \sum_{k=1}^{\infty} \frac{1}{k} g(x^k) \right], \quad (2.17)$$

$$g(x) = \frac{(1-x^3)^4}{(1-x)^4(1-x^4)^2} - \frac{1-x^4+x^8}{(1-x^4)^2}. \quad (2.18)$$

---

<sup>5</sup>Recently, it has been shown that a large class of 3d mirror symmetry, and its  $SL(2, \mathbb{Z})$  generalization, can be derived from 3d Aharony duality [46–48]. Thus, it is not surprising that these two classes of dualities share common examples.

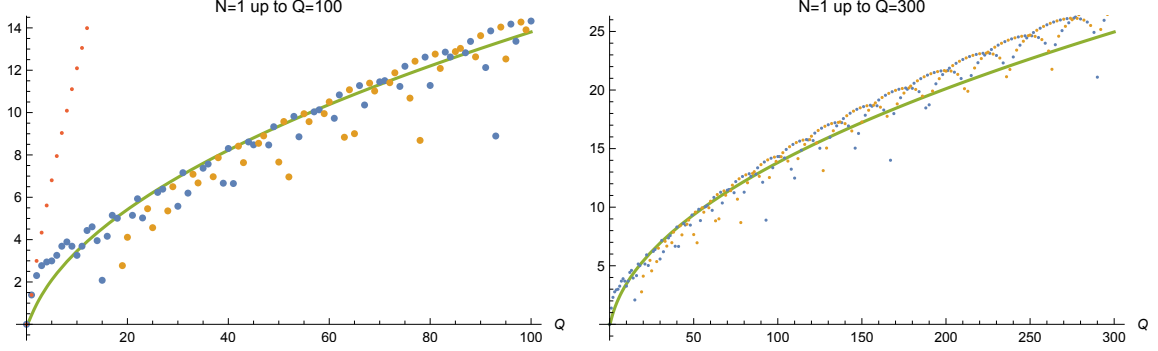


**Figure 1.**  $\log I_{N=1}(Q)$  (blue & orange dots) vs  $S(Q)$  (green line) up to  $x^{100}$  on the left and up to  $x^{300}$  on the right. Blue and orange dots represent coefficients with positive and negative signs, respectively. In the left plot, the small red dots indicate the graviton spectrum derived from the gravity side. While  $\log I_{N=1}$  fits relatively well with  $S$  for  $Q < 100$ , it deviates from  $S$  for higher  $Q$ .

The  $N = 1$  and graviton indices are then evaluated as follows:

$$\mathcal{I}_{N=1}(x) = 1 + 4x + 10x^2 + 16x^3 + \dots, \quad (2.19)$$

$$\mathcal{I}_{N=\infty}^{\text{graviton}}(x) = 1 + 4x + 20x^2 + 76x^3 + \dots, \quad (2.20)$$

which coincide up to  $x^1$ . We will comment on the meaning of the deviation at higher orders when we examine the indices for  $N = 2, 3$  in the next subsection. Notice that any scalar operator of dimension  $1/2$ , contributing to the index by  $x$ , is free according to the superconformal algebra [51]. In the present case, we see  $4x$  in the expansion of the  $N = 1$  index, which is consistent with the fact that the dual theory is described by a pair of a free hyper and a twisted hyper, or equivalently, four free chirals. For reference, the complete index data can be found in appendix A.

As anticipated, this agreement with the analytic curve is not permanent. One can reach much higher order of the expansion using the dual free hypermultiplet description, whose index merely that of four free chirals:

$$\mathcal{I}_{N=1}^{\text{dual}}(x) = \exp \left[ \sum_{k=1}^{\infty} \frac{1}{k} \frac{4x^k - 4x^{3k}}{1 - x^{4k}} \right]. \quad (2.21)$$

The result is shown in the right plot of Figure 1, which shows significant deviation at large  $Q$ . Despite such deviation, we observe that the leading large- $N$  free energy (2.14) is good enough to approximate the growth of the  $N = 1$  index for  $Q < 100$ , meaning that the states associated with this leading contribution dominates in this charge range. In the following discussions, we focus on the same charge range, which thus allows us to use the large- $N$  expression to approximate the  $N = 1$  index. This approximation proves useful when examining other examples in the subsequent subsections.

## 2.2 $N = 2, 3$

Next, we move on to the  $N = 2, 3$  cases, which are our main examples. Again, one can compute the indices using the factorization formula (2.7) and compare them with the large-

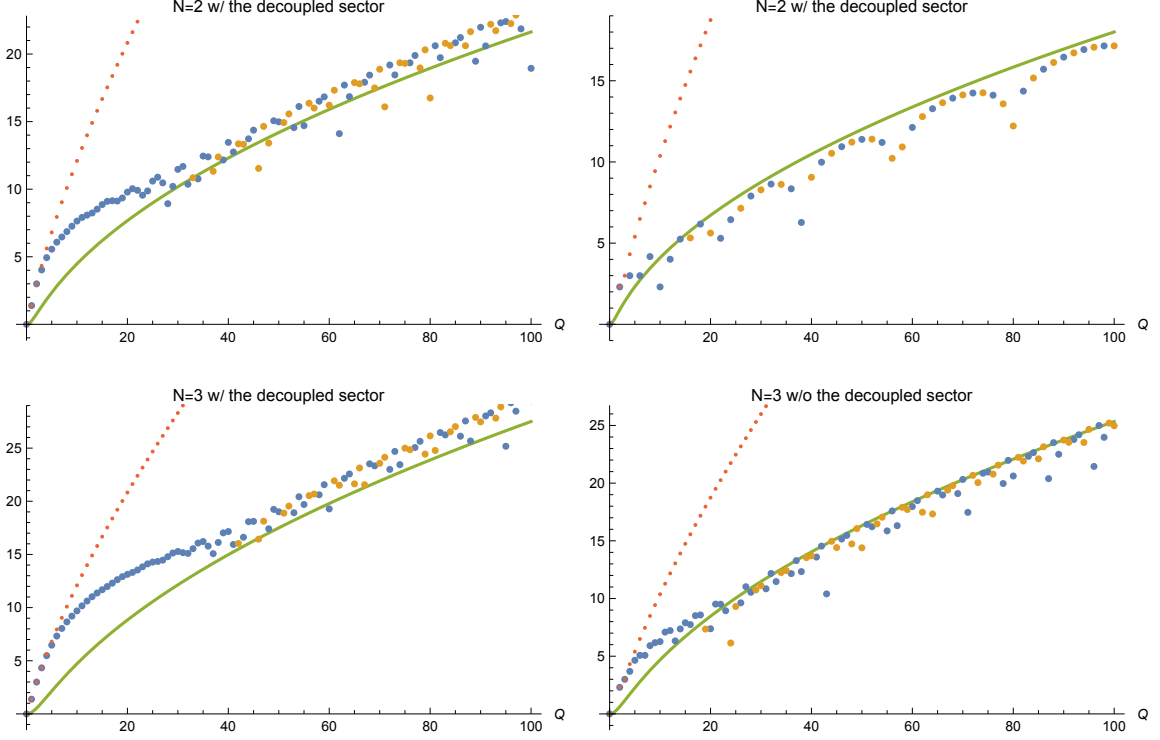


**Figure 2.**  $\log I_{N=2,3}(Q)$  (blue & orange dots) vs  $S(Q)$  (green line) on the left and  $\log I_{N=2,3}/I_{N=1}(Q)$  (blue & orange dots) vs  $S_{\text{int}}(Q)$  (green line) on the right, both up to  $x^{100}$ . Blue and orange dots represent coefficients with positive and negative signs, respectively, while the small red dots indicate the graviton spectrum derived from the gravity side. The left and right plots in each line differ by the decoupled hypermultiplets, whose index contribution is the same as  $I_{N=1}$ .

$N$  curves. See the left plots of Figure 2.

Similarly to the 4d  $\mathcal{N} = 4$  SYM case [11, 12], we observe a clear transition, around  $x^{20}$  and  $x^{30}$  for  $N = 2, 3$ , respectively, after which both the coefficient sign (+: blue, -: orange) and the logarithm of its absolute value begin to oscillate. Furthermore, the growth of the number of states fits well with the analytic curve (green) obtained from the large- $N$  analysis, up to some overall shift. Thus, it is natural to identify this region as black hole-dominant.

On the other hand, before the transition, where there is no oscillation, we expect this region is dominated by gravitons. For comparison, we again include the graviton index derived from the gravity side in the plots (red dots). The three indices are then given by

$$\mathcal{I}_{N=2}(x) = 1 + 4x + 20x^2 + 56x^3 + 139x^4 + 260x^5 + \dots, \quad (2.22)$$

$$\mathcal{I}_{N=3}(x) = 1 + 4x + 20x^2 + 76x^3 + 239x^4 + 644x^5 + \dots, \quad (2.23)$$

$$\mathcal{I}_{N=\infty}^{\text{graviton}}(x) = 1 + 4x + 20x^2 + 76x^3 + 274x^4 + 900x^5 + \dots, \quad (2.24)$$

where a few lowest order terms of the  $N = 2, 3$  indices coincide with those of the graviton index. We again see  $4x$  in the index expansion, indicating that there are four decoupled

free chirals. For reference, the complete index data can be found in appendix A.

The fact that the indices agree with that of gravitons only at the lowest few orders even in the graviton-dominant region implies important lessons. From the field theory perspective, the deviation arises due to the trace relation originating from the finite rank of the gauge group, whereas from the gravity perspective, it is attributed to the formation of giant gravitons. The giant gravitons are gravitons carrying large angular momenta in the near horizon geometries, which behave like extended branes [52]; in M-theory on  $\text{AdS}_4 \times S^7$ , they correspond to M5-branes wrapping supersymmetric cycles in  $S^7$ . Recently, it has been proposed that supersymmetric indices admit expansions in terms of giant graviton contributions as follows [53]:

$$\frac{Z_N(x; \vec{y})}{Z_\infty(x; \vec{y})} = 1 + \sum_{k=1}^{\infty} x^{kN} \hat{Z}_k(x, \vec{y}) \quad (2.25)$$

where  $x$  is a particular symmetry fugacity, and  $\vec{y}$  are the others. One can see that the giant graviton contributions encode the systematic corrections to the graviton index at  $N = \infty$  to recover the finite- $N$  index, which are thus the source of the discrepancy between the two indices. As far as we are aware of, the explicit form of the giant graviton contributions for the superconformal index of the 3d  $\mathcal{N} = 8$  SCFT at finite  $N$  is not known yet.

As noted earlier, a theory with  $N > 1$  also includes a decoupled pair of a hyper and a twisted hypermultiplets, which should correspond to BPS gravitons. Thus, if we are interested in black hole states, we should look at the interacting sector, whose index can be obtained by dividing its index by that of  $N = 1$ . For comparison with the large- $N$  analytic curve, we should also subtract the contribution of the decoupled sector from the large- $N$  free energy (2.14). Since we have observed that (2.14) also explains the growth of the  $N = 1$  index for  $Q < 100$ , the logarithm of the index of the interacting sector can be approximated as follows:

$$\log \mathcal{I}_N / \mathcal{I}_{N=1} = -(\mathcal{F}_N - \mathcal{F}_{N=1}) = -i \frac{4\sqrt{2} \left( N^{\frac{3}{2}} - 1 \right) (\pi i + \beta)^2}{24 \beta}, \quad (2.26)$$

where the scaling factor  $N^{\frac{3}{2}}$  is shifted to  $N^{\frac{3}{2}} - 1$ . Thus, the entropy of the interacting sector is obtained by replacing  $N^{\frac{3}{2}}$  by  $N^{\frac{3}{2}} - 1$ :

$$S_{\text{int}}(Q; N^{\frac{3}{2}}) = S(Q; N^{\frac{3}{2}} - 1), \quad (2.27)$$

where  $S$  on the right hand side is given by (2.15). In this way, we can compare the logarithm of the exact indices and the large- $N$  entropy for the interacting sector. The results for  $N = 2, 3$  are shown in the right plots of Figure 2. Notice that the agreement between the two becomes more precise; in particular, the transition point appears earlier than the original index including the decoupled sector. This supports the interpretation that the decoupled sector contains only graviton states; by dividing the index by that of the decoupled sector, i.e., the  $N = 1$  index, we remove part of the graviton contribution, making the black hole contribution more manifest in the resulting index.

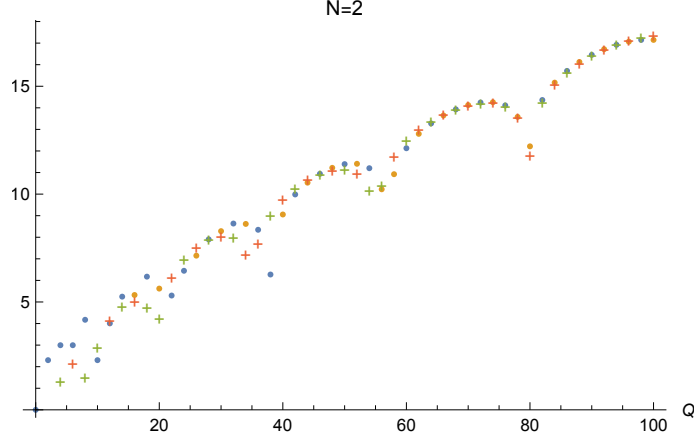


**Figure 3.**  $\log I_{N=2}/I_{N=1}(Q)$  (blue & orange dots) vs  $\tilde{S}(Q; \gamma = 0.53, \delta = -0.4)$  (green & red crosses) up to  $x^{100}$ . Blue dots and green crosses correspond to coefficients with the positive sign, whereas orange dots and red crosses correspond to coefficients with the negative sign. There is good agreement between the dots and the crosses in the oscillating region for large  $Q$ .

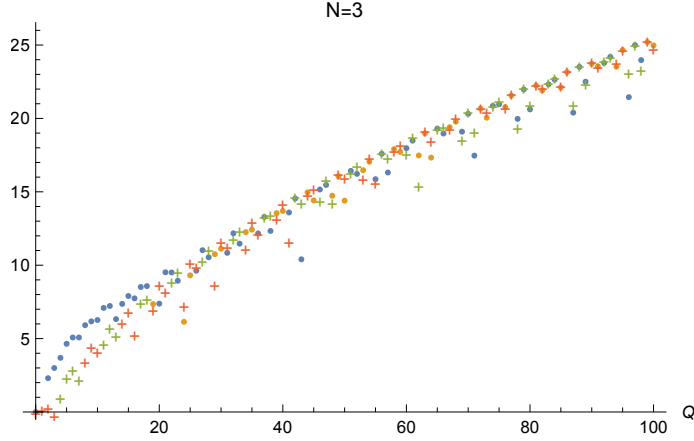


**Figure 4.**  $\log I_{N=3}/I_{N=1}(Q)$  (blue & orange dots) vs  $\tilde{S}(Q; \gamma = 0.95, \delta = 0.2)$  (green & red crosses) up to  $x^{100}$ . Blue dots and green crosses correspond to coefficients with the positive sign, whereas orange dots and red crosses correspond to coefficients with the negative sign. Other than the points for small  $Q$  and those corresponding to  $\cos[\dots] \approx 0$  in (2.29), whose logarithm diverges, there is good agreement between the dots and the crosses.

Moreover, we observe an interesting sinusoidal pattern from the  $N = 2$  index after subtracting the decoupled sector contribution. See the top-right plot in Figure 2. Similar behavior has been observed in the 4d  $\mathcal{N} = 4$  SYM case and can be explained by the complex nature of the large- $N$  saddle point [12]. It turns out our case can also be explained by the same origin. Since a complex saddle must come in pair with its complex conjugate, the actual contribution to the index is  $e^{S_{\text{int}}} + e^{S_{\text{int}}^*}$ , whose logarithm is given by

$$\log \left[ e^{S_{\text{int}}} + e^{S_{\text{int}}^*} \right] \approx \text{Re } S_{\text{int}} + \log |\cos [\text{Im } S_{\text{int}} + \dots]| + \dots, \quad (2.28)$$

where the oscillation primarily depends on the imaginary part of the complexified entropy.

For better visibility of the comparison, we introduce fitted entropy  $\tilde{S}$  with two  $O(1)$  parameters  $\gamma$  and  $\delta$ :

$$\tilde{S}(Q; \gamma, \delta) = \text{Re } S_{\text{int}}(Q) + \log \left| \cos \left[ \text{Im } S_{\text{int}}(Q) + \frac{\pi}{2}(Q-1) - \gamma \right] \right| + \delta \quad (2.29)$$

where  $\frac{\pi}{2}(Q-1)$  is introduced to reflect the correct period of the sign oscillation of the index. With this minimal modification and some chosen values of  $\gamma$  and  $\delta$ ,<sup>6</sup> we observe impressive agreement between the exact index and the large- $N$  prediction, unless  $Q$  is too small. See Figure 3. Furthermore, although such a sinusoidal pattern is not manifest in the  $N=3$  case, the large- $N$  entropy with the minimal modification also showcases the impressive agreement with the exact index for  $N=3$  as well. See Figure 4. Note that most of the deviation arises when  $Q$  is small or when the cosine term in (2.29) approaches 0, where the logarithm diverges and subleading corrections become significant.

### 2.2.1 Complex- $\beta$ phase diagram

So far, we have focused on the behavior of the index as a function of  $Q$ , i.e., its micro-canonical aspect. However, it is also important to understand the canonical aspect by considering the index as a function of  $\beta$ . Recall that the key feature distinguishing the black hole-dominant region from the graviton-dominant region is the presence of the sign oscillation, which arises from the definition of the index, where bosonic and fermionic states contribute with opposite signs. Due to this sign difference, it was long believed that the index, as a canonical quantity, could not capture the large entropy associated with black holes. This is true to some extent when  $\beta$  is real, but not when  $\beta$  is allowed to take complex values. Indeed, this is one of the most important lessons from the large  $N$  analysis, which successfully reproduces the black hole entropy assuming complex  $\beta$  [4–6, 8], whereas real  $\beta$  leads to the graviton index of  $O(1)$  in the large- $N$  limit [2, 20].

Here, we find that complex  $\beta$  plays an important role in the finite- $N$  computation as well. First, we introduce the *complex- $\beta$  phase diagram* of the index for the interacting sector by evaluating its absolute value  $|\mathcal{I}_N/\mathcal{I}_{N=1}(\beta)|$  as  $\beta$  varies over the complex plane. We have observed that, obviously,  $|\mathcal{I}_N/\mathcal{I}_{N=1}(\beta)|$  decreases as  $\text{Re } \beta$  increases, which is expected since  $x = e^{-\beta/2}$ , and larger values of  $\beta$  suppress more terms in the series expansion. However, richer structure emerges when we compare different values of  $\theta \equiv \text{Im } \beta/2$ .

Recall the fact that the graviton-dominant region has the uniform sign, while the black hole-dominant region has alternating ones. This means that for nonzero  $\theta$ , the graviton contributions are diminished due to additional phases that lead to cancellations. In contrast, the black hole contributions will be amplified, as the original cancellations from alternating signs are disrupted. Thus, at large  $\beta$ , where the index primarily captures small- $Q$  states dominated by gravitons, the absolute value of the index should be maximized at  $\theta = 0$ . Indeed, we have found that this is the case; see the left plots of Figures 5 and 6, which are

---

<sup>6</sup>We do not aim to precisely determine the best-fitting values of  $\gamma$  and  $\delta$ , as our goal here is merely to demonstrate that the large- $N$  prediction already provides a good approximation for small  $N$ . The precise values of  $\gamma$  and  $\delta$  would become relevant when studying subleading corrections.

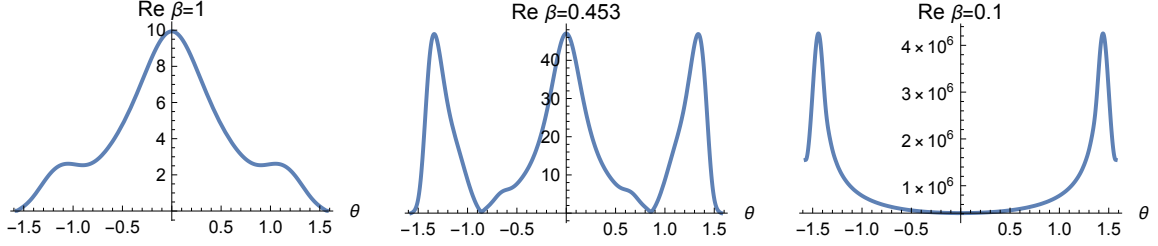


**Figure 5.**  $|\mathcal{I}_{N=2}/\mathcal{I}_{N=1}(\beta)|$  as a function of  $\theta = \text{Im } \beta/2$  when  $\text{Re } \beta = 1$  (left), 0.453 (center), 0.1 (right), respectively. For  $N = 2$ , the periodicity of  $\theta$  is  $\pi$ , half of the other cases because only even powers appear in the series expansion. The transition occurs when  $\beta = 0.453$  (center), where there are two peaks, up to sign, one at  $\theta = 0$  and the other at  $\theta = \pm 1.34$ .

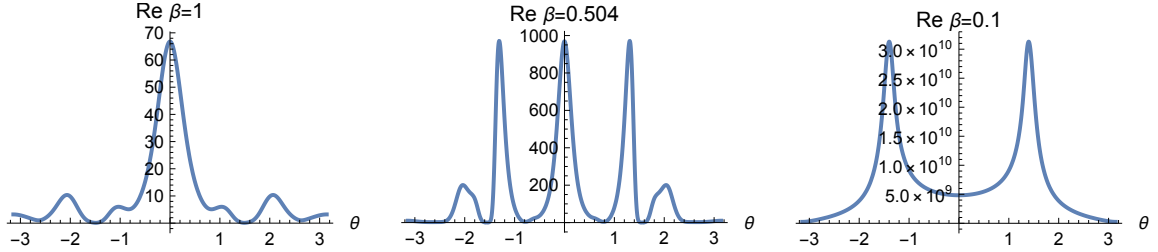


**Figure 6.**  $|\mathcal{I}_{N=3}/\mathcal{I}_{N=1}(\beta)|$  as a function of  $\theta = \text{Im } \beta/2$  when  $\text{Re } \beta = 1$  (left), 0.504 (center), 0.1 (right), respectively. The transition occurs when  $\beta = 0.504$ , where there are three peaks, up to sign, at  $\theta = 0, \pm 1.31, \pm 2.04$ .

drawn using the series expansion truncated at  $Q = 120$  for better precision. The two plots show the values of  $|\mathcal{I}_N/\mathcal{I}_{N=1}(\beta)|$  at fixed  $\text{Re } \beta = 1$  as a function of  $\theta$ , the imaginary part of  $\beta/2$ , for  $N = 2, 3$ , respectively. As expected, they exhibit the maximal peak at  $\theta = 0$ . At small  $\beta$ , on the other hand, the index mainly captures large- $Q$  states dominated by black hole states, whose contribution should be maximized at nonzero  $\theta$ . See the right plots of Figures 5 and 6, displaying  $|\mathcal{I}_N/\mathcal{I}_{N=1}(\beta)|$  at fixed  $\text{Re } \beta = 0.1$ . The maximum peaks arise around  $\theta = \pm 1.44$  for  $N = 2$  and at  $\theta = \pm 1.40$  for  $N = 3$ , both of which are nonzero as anticipated.<sup>7</sup>

This means that there is a transition at some intermediate value of  $\text{Re } \beta$ , where a peak at nonzero  $\theta$  overtakes the peak at  $\theta = 0$ . This can be interpreted as a type of graviton-black hole transition for the interacting sector, as we expect that a peak at nonzero  $\theta$  is primarily associated with the black hole contribution, whereas the peak at  $\theta = 0$  is associated with that of gravitons. We have obtained these transition-point values of  $\text{Re } \beta$  numerically, which are 0.453 for  $N = 2$  and 0.504 for  $N = 3$ .  $|\mathcal{I}_N/\mathcal{I}_{N=1}(\beta)|$  at these points are shown in the center plots of Figures 5 and 6, where the peaks at nonzero  $\theta$ ,  $\theta = \pm 1.34$  for  $N = 2$  and  $\theta = \pm 1.31$  for  $N = 3$ , match the peak at  $\theta = 0$ .

<sup>7</sup>The peak values at  $\beta = 0.1$  are not saturated when evaluated using the series expansion truncated at  $Q = 120$ . However, their precise values are not our primary focus and not pursued here; clearly, more accurate results could be obtained by including additional terms in the series. In contrast, the results presented at other values of  $\beta$  are all saturated.

Furthermore, for  $N = 3$ , if  $\text{Re } \beta$  is not too small so that the peak at the first nonzero  $\theta$  does not dominate all others, one can observe the crucial fact that there are actually multiple peaks at nonzero  $\theta$ . This suggests the existence of two distinct collections of states whose sign oscillations have different periods in  $Q$ . Furthermore, they should be associated with different entropies because, as seen in (2.29), the sign oscillation of the index is governed by the imaginary part of the complex-valued entropy. From (2.29), one can estimate the peak value of  $\theta$  corresponding to the known black hole entropy. As discussed, the index of the interacting sector is given by

$$\mathcal{I}_N / \mathcal{I}_{N=1} = \sum_{Q=0}^{\infty} I(Q) x^Q \quad (2.30)$$

where  $I(Q)$  includes sign. In Figure 4, we have seen that  $I(Q)$  can be approximated by the leading large- $N$  entropy

$$I(Q) \approx e^{\tilde{S}} = e^{\text{Re } S_{\text{int}}(Q) + \delta} \cos \left[ \text{Im } S_{\text{int}}(Q) + \frac{\pi}{2}(Q - 1) - \gamma \right]. \quad (2.31)$$

In order to minimize the cancellation between different  $Q$  so that we have a peak in the phase diagram, the phase difference between adjacent values of  $Q$ , including that of  $x^Q = |x^Q|e^{-i\theta Q}$ , should be a multiple of  $2\pi$ :

$$\pm \left( \frac{\Delta \text{Im } S_{\text{int}}(Q)}{\Delta Q} + \frac{\pi}{2} \right) - \theta = 2\pi k, \quad k \in \mathbb{Z}. \quad (2.32)$$

Given that the period of  $\theta$  is  $2\pi$ , we simply get

$$\theta = \pm \left( \frac{\Delta \text{Im } S_{\text{int}}(Q)}{\Delta Q} + \frac{\pi}{2} \right). \quad (2.33)$$

Since  $\Delta \text{Im } S_{\text{int}}(Q) / \Delta Q$  is not a constant, we need to determine which values of  $Q$  dominantly contribute. Recall that, from the Legendre transformation, the relation between  $\beta$  and  $Q$  is determined as (2.16), which tells us the dominantly contributing value of  $Q$  for a given  $\beta$ . For example, at the transition-point for  $N = 3$ ,  $\text{Re } \beta = 0.504$ , the dominant  $Q$  is around 45, where the least interfering value of  $\theta$ , determined by (2.33), is  $\pm 1.33$ . This value is close enough to the one we obtained from the numerical index data,  $\theta = \pm 1.31$ , given that the latter includes other contributions such as gravitons. Therefore, the peak at  $\theta = \pm 1.31$  should correspond to the known black hole solution, whose entropy is governed by  $\tilde{S}$ .

As a further consistency check, we also plot the complex- $\beta$  phase diagrams for the black hole index governed by  $\tilde{S}$  in (2.31) and for the graviton index (2.17), in place of the  $N = 3$  index data. As anticipated, the black hole phase diagram exhibits a single peak at nonzero  $\theta$  (modulo sign), while the graviton phase diagram shows a peak at  $\theta = 0$ . See Figure 7.

Most importantly, the small peak at  $\theta = \pm 2.04$  of the center plot in Figure 6 corresponds to neither of these, strongly suggesting that it is associated with a different type of gravitational solution. While we approximate the index using the large- $N$  entropy  $\tilde{S}$  in (2.31), generically, the index would get contributions from multiple saddles, labeled by  $a$ :

$$\mathcal{I}(\beta) = \sum_a \sum_Q I_a(Q) e^{-\beta Q} \quad (2.34)$$



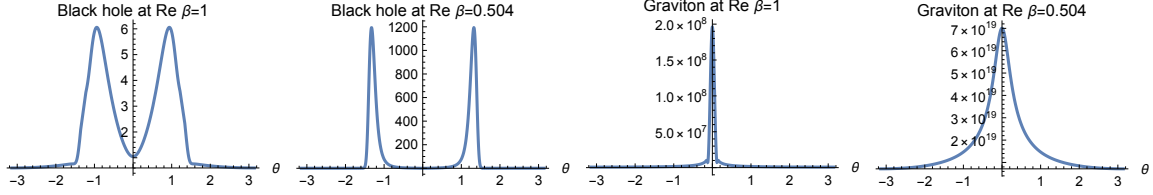


**Figure 7.** The left two are the black hole indices at  $\beta = 1$  and  $\beta = 0.504$  estimated from the large- $N$  entropy  $\tilde{S}$ , given by (2.29). The right two are the graviton indices  $\mathcal{I}_{N=\infty}^{\text{graviton}}/\mathcal{I}_{N=1}$  at  $\beta = 1$  and  $\beta = 0.504$ .

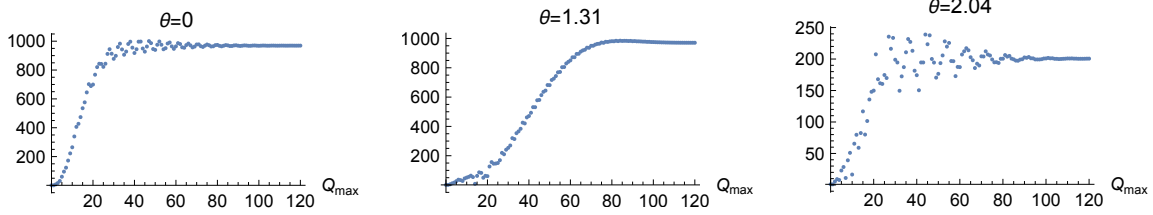


**Figure 8.**  $|\mathcal{I}_{N=3}/\mathcal{I}_{N=1}(\beta)|$  for different truncation orders,  $Q_{\text{max}}$ , evaluated at the three peaks ( $\theta = 0$  (left),  $\theta = 1.31$  (center),  $\theta = 2.04$  (right)) at the transition point ( $\text{Re } \beta = 0.504$ ).

with

$$I_a(Q) = e^{S_a(Q)} + e^{S_a^*(Q)} \sim e^{\text{Re } S_a(Q)} \cos \text{Im } S_a(Q) \quad (2.35)$$

where  $S_a(Q)$  includes all the corrections, such as  $\frac{\pi}{2}(Q - 1)$  in the argument of the cosine factor and other  $O(1)$  shifts in (2.31). The location of the peak in the phase diagram associated with saddle  $a$  is then given by

$$\theta_a = \pm \frac{\Delta \text{Im } S_a(Q)}{\Delta Q}. \quad (2.36)$$

In other words, our peak at  $\theta = \pm 2.04$  indicates that there should be a saddle where  $\frac{\Delta \text{Im } S_a(Q)}{\Delta Q} \approx 2.04$  for dominantly contributing  $Q$ . Although its precise nature remains unclear, we will see in Section 3 that this peak is related to a particular Higgs vacuum with vortex excitations, which can also be interpreted as a solution to the Bethe ansatz equations (BAEs) associated with 3d supersymmetric partition functions [29]. This may hint at a connection between the peak at  $\theta = \pm 2.04$  and a gravitational solution distinct from the well-known graviton gas or black hole configurations, as there is evidence that a particular set of BAE solutions corresponds to the contribution of a specific gravitational background, at least in the unrefined limit [37].

We conclude this subsection with one final comment. The series expansion of the index we have used to analyze the complex- $\beta$  phase diagram is truncated at  $Q = 120$ . Therefore, it is important to verify whether this truncated series includes a sufficient number of terms to reliably estimate  $|\mathcal{I}_N/\mathcal{I}_{N=1}(\beta)|$ , especially at the transition points. To this end, we have evaluate  $|\mathcal{I}_N/\mathcal{I}_{N=1}(\beta)|$  using various truncation orders in  $Q$  and confirmed that keeping terms up to  $Q = 120$  yield results sufficiently close to the saturated values, except at

$\beta = 0.1$ , which requires additional terms in the expansion. Nevertheless, the accurate values at other  $\beta$  are enough for our purposes, so we do not pursue further refinement here. As an example, we provide the case for  $N = 3$  at the transition point,  $\beta = 0.504$  in Figure 8.

### 2.3 $N = 4, 5$

Our last examples are  $N = 4, 5$ . However, these cases require significantly higher computational costs compared to the  $N = 2, 3$  cases due to larger number of possible Young diagrams, making it difficult to evaluate the indices to sufficiently high orders. Fortunately, our primary interest lies in the overall growth of the index rather than in the precise coefficients, which allows for approximations that reduce the computational burden.

To this end, we first note that the vortex part (2.9) is expressed as a series in  $w$ , the vorticity fugacity, rather than in  $x$ . Thus, we need to determine the maximum vorticity contributing to a given power of  $x$ , say  $x^n$ , so that we can truncate the vorticity sum at an appropriate order. One can verify that the largest vorticity contributing to  $x^n$  is  $n$ . Namely, to compute the index up to  $x^{100}$  as we did in the previous subsections, we require vortex contributions up to vorticity 100.

On the other hand, if we are concerned with the scaling of the overall growth rather than the precise index, the contributions from high vorticity may be less significant. The reason is that, as we have seen in the  $N = 2, 3$  cases, if  $Q$  is not too small, the dominant contribution to the index comes from the black hole states, whose contribution can be approximated using the large- $N$  free energy (2.5), which is symmetric under the permutations of  $\Delta_i$ . Thus, the entropy obtained by the Legendre transformation will also be symmetric under the permutations of charges  $Q_i$ , indicating that for large enough charges  $Q_i$ , the primary contribution will be attributed to equal charge sector. As explained earlier, one of the  $Q_i$  counts the monopole flux, or, from the gapped theory perspective, the vortex charge. Thus, for given  $Q$ , the dominant vorticity would be  $Q/4$  if we ignore the angular momentum  $j$  for the moment so that  $Q \approx Q_1 + Q_2 + Q_3 + Q_4$ . Namely, the vortex contributions at vorticity  $n/4$  and nearby would be sufficient to capture the overall growth of the index up to  $x^n$ ; and it becomes even lower if we take into account the nonzero angular momentum required by the charge relation for a BPS black hole [54].

Indeed, we have tested the approximation of the  $N = 2, 3$  indices up to  $x^{100}$  by truncating vortex contributions at different vorticities 67, 50, and 33, corresponding to  $2/3$ ,  $1/2$ , and  $1/3$  of the maximum vorticity required for the exact computation. The results are shown in Figure 9. We observe that the approximation with vorticity up to 67 is nearly indistinguishable from the exact index on a logarithmic scale. The approximation with vorticity up to 50 is also quite accurate, while truncating at 33 results in noticeable deviations, though the overall growth remains qualitatively similar.

Based on this idea, we aim to evaluate the indices for  $N = 4, 5$  using truncated vortex contributions, as the exact results are more difficult to obtain due to the high computational cost. We calculate the indices keeping the vortex contributions up to vorticity 67 and 50 for  $N = 4, 5$ , respectively, which should be more than enough to capture the overall scaling of the indices, according to the comparison made for  $N = 2, 3$ . The results are shown in Figures 10 and 11, where the latter includes the correction by the cosine factor

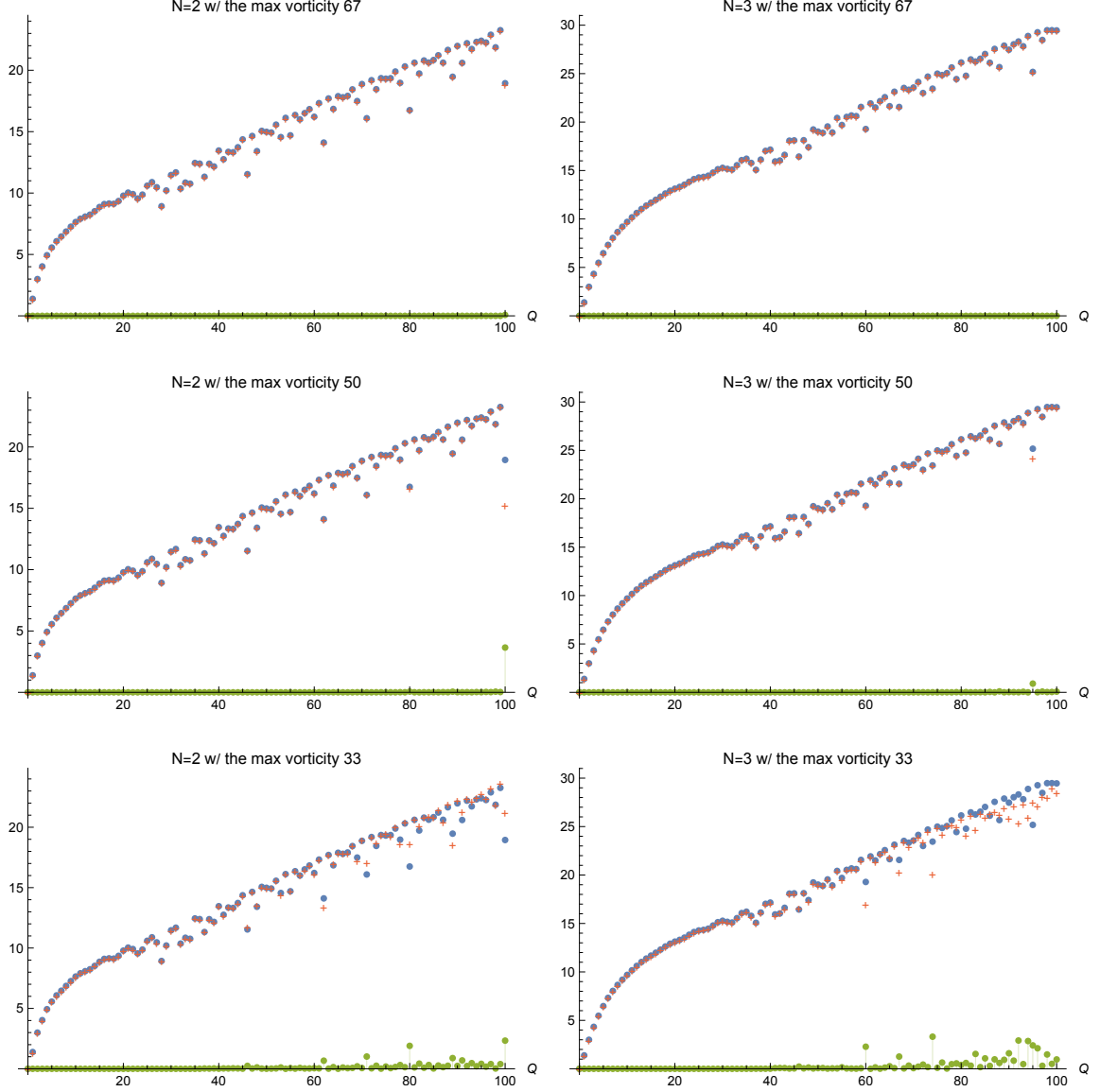


**Figure 9.** Exact  $\log I_N(Q)$  (blue dots) vs those with truncated vortex contributions (red crosses) for  $N = 2$  on the left and for  $N = 3$  on the right. The green dots represent the difference between the exact value and the approximated value with the truncation. We have tested the maximal vorticity of 67, 50, and 33, which are  $2/3$ ,  $1/2$ , and  $1/3$  of the required value when computing the index up to  $Q = 100$ , respectively.

in (2.29) as well. As expected, we observe good agreement between the large- $N$  curves and the approximated indices computed using truncated vortex contributions. However, it remains unclear whether this level of precision is sufficient for analyzing the complex- $\beta$  phase diagram for  $N = 4, 5$ , and we thus leave this investigation for future work.

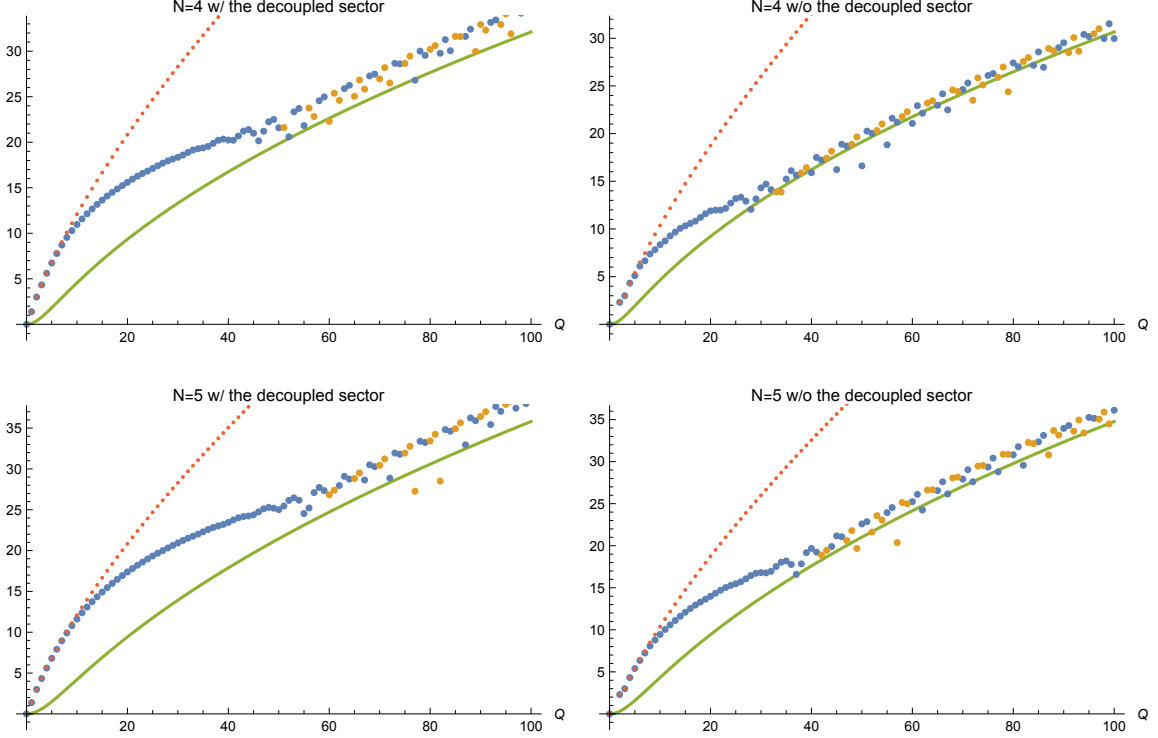


**Figure 10.**  $\log I_{N=4,5}(Q)$  (blue & orange dots) vs  $S(Q)$  (green line) on the left and  $\log I_{N=4,5}/I_{N=1}(Q)$  (blue & orange dots) vs  $S_{\text{int}}(Q)$  (green line) on the right, both up to  $x^{100}$ . The  $I_N(Q)$  used here is an approximate result, obtained by keeping vortex contributions up to vorticity 67 for  $N = 4$  and up to 50 for  $N = 5$ . As before, blue and orange dots represent coefficients with positive and negative signs, respectively, while the small red dots indicate the graviton spectrum derived from the gravity side. The left and right plots in each line differ by the decoupled hypermultiplets, whose index contribution is the same as  $I_{N=1}$ .

### 3 BPS indices on Higgs vacua of the 3d ADHM with a single flavor

As explained in the previous section, the superconformal index can be written as a sum of indices over the discrete Higgs vacua of the theory with generic real masses. Importantly, this structure is not unique to the superconformal index but also appears in other types of supersymmetric partition functions on manifolds that are  $S^1$  fibered over  $S^2$  [22–30]. A notable example is the topologically twisted index [28], which exhibits the same structure. The building blocks in both cases are the same: the vortex partition function on  $\mathbb{R}^2 \times S^1$  (including perturbative contribution). The only difference lies in how these building blocks are glued together. As we have seen, for the superconformal index, we glue two vortex partition functions related by  $f \leftrightarrow f^{-1}$  where  $f$  collectively denotes all the symmetry fugacities, while  $m$ , collectively denoting symmetry fluxes, remains invariant. In contrast, for the topologically twisted index, we glue two vortex partition functions related by  $m \leftrightarrow -m$ , whereas  $f$  remains invariant [29].

In fact, the topologically twisted index admits an alternative formulation, called Bethe ansatz formalism, which expresses the index as a sum over solutions to the so-called Bethe

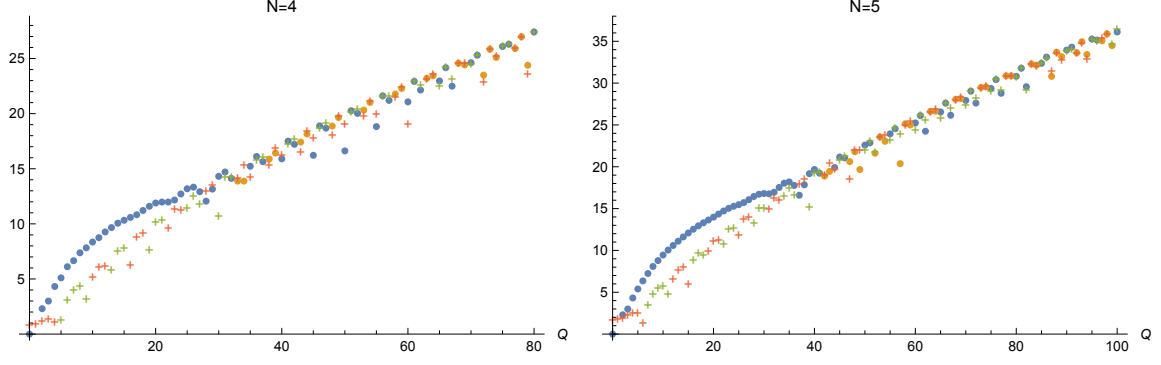


**Figure 11.**  $\log I_{N=4}/I_{N=1}(Q)$  (blue & orange dots) vs  $\tilde{S}(Q; \gamma = 1.03, \delta = 1.1)$  (green & red crosses) on the left and  $\log I_{N=5}/I_{N=1}(Q)$  (blue & orange dots) vs  $\tilde{S}(Q; \gamma = 1.24, \delta = 1.9)$  (green & red crosses) on the right, both up to  $x^{100}$ . Blue dots and green crosses correspond to coefficients with the positive sign, whereas orange dots and red crosses correspond to coefficients with the negative sign. Other than the points for small  $Q$  and those corresponding to  $\cos[\dots] \approx 0$  in (2.29), whose logarithm diverges, there is good agreement between the dots and the crosses.

ansatz equation (BAE), the equation of motion associated with the twisted superpotential of the theory compactified on  $S^1$  [28]. For the ADHM quiver, such BAE solutions coincide precisely with the discrete Higgs vacua discussed earlier. The key point is that there is evidence suggesting that each BAE solution, or a certain set of solutions, corresponds to a particular holographic dual gravity solution. For instance, for the 4d  $\mathcal{N} = 4$  SYM index with equal angular velocities, there exist known BAE solutions, called the Hong-Liu solutions, whose contribution in the large- $N$  limit match the standard Euclidean black hole solutions and their orbifolds [37]. However, this correspondence is subtle, as it no longer holds when the angular velocities are unequal [55].

Since we are discussing the unrefined index, it is natural to ask whether each Higgs vacuum, viewed as a version of a BAE ansatz solution, has any gravitational interpretation in the large- $N$  limit. Unfortunately, this is difficult to answer, as we currently lack the tools to evaluate the large- $N$  limit of the index for an individual Higgs vacuum. Instead, we aim to analyze the complex- $\beta$  phase diagram of the index on each Higgs vacuum to see if there is any relation between the peaks in the phase diagrams and the Higgs vacua of theory.

One immediate difficulty is that the index at an individual Higgs vacuum does not have well-defined unrefined limit. For example, the  $U(3)$  ADHM with a single flavor has three

Higgs vacua, for which the index reads as follows:

$$\begin{array}{|c|} \hline \square \\ \hline \square \\ \hline \end{array} : -q^{\frac{1}{2}} \frac{t^{\frac{1}{2}} z^4}{z - z^{-1}} + q \frac{t^{-1} z - z^4 (w + w^{-1}) - t z^5 (z^2 + 1 + z^{-2})}{z - z^{-1}} + \dots, \quad (3.1)$$

$$\begin{array}{|c|c|} \hline \square & \square \\ \hline \end{array} : 1 + q^{\frac{1}{2}} \left[ t^{-\frac{1}{2}} (w + w^{-1}) + t^{\frac{1}{2}} (z^3 + 2z + 2z^{-1} + z^{-3}) \right] \\ + q \left[ t^{-1} (2w^2 + 1 + 2w^{-2}) + (w + w^{-1}) (z^3 + 3z + 3z^{-1} + z^{-3}) \right. \\ \left. + t (z^6 + 2z^4 + 5z^2 + 5 + 5z^{-2} + 2z^{-4} + z^{-6}) \right] + \dots, \quad (3.2)$$

$$\begin{array}{|c|c|c|} \hline \square & \square & \square \\ \hline \end{array} : q^{\frac{1}{2}} \frac{t^{\frac{1}{2}} z^{-4}}{z - z^{-1}} - q \frac{t^{-1} z^{-1} - z^4 (w + w^{-1}) - t z^{-5} (z^2 + 1 + z^{-2})}{z - z^{-1}} + \dots, \quad (3.3)$$

whose sum results in the complete superconformal index:

$$\mathcal{I}_{N=3}(w, z, t, q) = 1 + q^{\frac{1}{2}} \left[ t^{-\frac{1}{2}} (w + w^{-1}) + t^{\frac{1}{2}} (z + z^{-1}) \right] \\ + q \left[ 2t^{-1} (w^2 + 1 + w^{-2}) + 2 (w + w^{-1}) (z + z^{-1}) + 2t (z^2 + 1 + z^{-2}) \right] + \dots \quad (3.4)$$

One can see that the indices for  $\begin{array}{|c|c|c|} \hline \square & \square & \square \\ \hline \end{array}$  and  $\begin{array}{|c|c|c|} \hline \square & \square & \square \\ \hline \end{array}^T$ , which are symmetric under  $z \leftrightarrow z^{-1}$ , include a factor of  $(z - z^{-1})^{-1}$ , which diverges in the limit  $z \rightarrow 1$ . The origin of this factor is zero modes of an adjoint field at the corresponding Higgs vacua, whose contribution should diverge in the massless limit. This is not surprising because we have *discrete* Higgs vacua only when real masses are nonzero, while they become continuous vacuum moduli space in the massless limit.

Obviously, such zero modes are not part of the BPS spectrum in the massless limit leading to the SCFT. Namely, they must be paired up to form a long multiplet, whose combined contribution to the index vanishes. We find that certain combinations of the Higgs vacuum indices yield those with integer coefficients, where all the divergent contributions from the zero modes cancel out. Here are some examples for low values of  $N$ :

$$N = 2 : \begin{array}{|c|} \hline \square \\ \hline \end{array} + \begin{array}{|c|c|} \hline \square & \square \\ \hline \end{array}, \quad (3.5)$$

$$N = 3 : \begin{array}{|c|} \hline \square \\ \hline \square \\ \hline \end{array} + \begin{array}{|c|c|c|} \hline \square & \square & \square \\ \hline \end{array}, \quad \begin{array}{|c|c|} \hline \square & \square \\ \hline \end{array} \quad (3.6)$$

$$N = 4 : \begin{array}{|c|} \hline \square \\ \hline \square \\ \hline \square \\ \hline \end{array} + \begin{array}{|c|c|c|c|} \hline \square & \square & \square & \square \\ \hline \end{array}, \quad \begin{array}{|c|c|} \hline \square & \square \\ \hline \square & \square \\ \hline \end{array} + \begin{array}{|c|c|} \hline \square & \square \\ \hline \square & \square \\ \hline \end{array} + \begin{array}{|c|c|c|} \hline \square & \square & \square \\ \hline \end{array}, \quad (3.7)$$

$$N = 5 : \begin{array}{|c|} \hline \square \\ \hline \square \\ \hline \square \\ \hline \square \\ \hline \end{array} + \begin{array}{|c|c|c|c|c|} \hline \square & \square & \square & \square & \square \\ \hline \end{array}, \quad \begin{array}{|c|c|} \hline \square & \square \\ \hline \square & \square \\ \hline \square & \square \\ \hline \end{array} + \begin{array}{|c|c|c|} \hline \square & \square & \square \\ \hline \square & \square & \square \\ \hline \end{array}, \quad \begin{array}{|c|c|} \hline \square & \square \\ \hline \square & \square \\ \hline \end{array} + \begin{array}{|c|c|c|} \hline \square & \square & \square \\ \hline \square & \square & \square \\ \hline \end{array} + \begin{array}{|c|c|c|} \hline \square & \square & \square \\ \hline \square & \square & \square \\ \hline \end{array}. \quad (3.8)$$

Note that all the combinations are symmetric under  $z \leftrightarrow z^{-1}$ , which is a symmetry of the SCFT. In fact, for  $N = 4, 5$ , the two linear Young diagrams corresponding to the partitions  $(N)$  and  $(1^N)$  are already free of zero-mode contributions individually, at least at low orders in  $q$ -expansion. Nevertheless, we sum their contributions to ensure symmetry under  $z \leftrightarrow z^{-1}$  for the refined index, as we do for the other combinations. We will call such

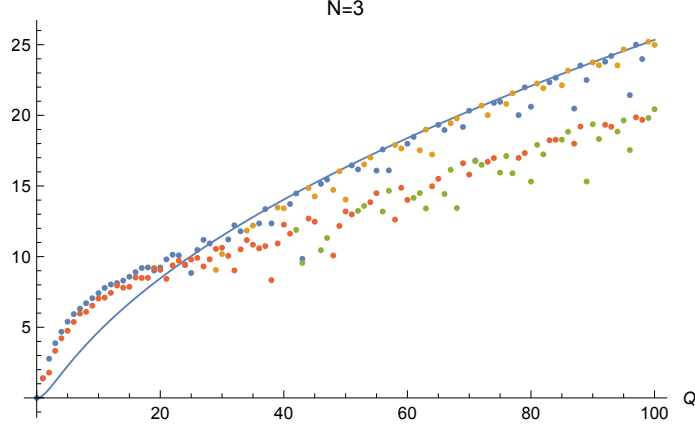


**Figure 12.** Two smooth Higgs vacuum indices for  $N = 3$ . The index corresponding to  $\square\square$  are represented by blue (positive sign) and orange (negative sign) dots, whereas the index corresponding to  $\square\square + \square\square^T$  are represented by green (positive sign) and red (negative sign) dots. While both of them exhibit oscillating behavior, only the index for  $\square\square$  matches the large- $N$  entropy  $\tilde{S}$  (blue line).

indices without zero-modes contributions *smooth* Higgs vacuum indices, in the sense that they admit a smooth unrefined limit.

One should note that the smooth indices also include states that become non-BPS in the SCFT limit. Nevertheless, it is possible that such accidental BPS states in the gapped vacua are subdominant, and each smooth Higgs vacuum index could still provide insight into the primary contribution to the SCFT index, or holographically, that into a possible gravity solution in connection with the BAE solutions.

In this sense, it is natural to ask whether the peaks in the complex- $\beta$  phase diagram we observed in the previous section are related to the smooth Higgs vacuum indices. The answer seems to be yes. We focus on the  $N = 3$  case since, for  $N = 2$ , there is only one smooth Higgs vacuum index for  $N = 2$ , which is nothing but the superconformal index, and for  $N = 4, 5$ , we only have approximate indices. For  $N = 3$ , there are two smooth Higgs vacuum indices: one corresponding to the Young diagram  $\square\square$  and the other given by the sum of the Higgs vacuum indices associated with  $\square\square$  and  $\square\square^T$ . The growth of each smooth Higgs vacuum index is shown in Figure 12.

Both smooth indices exhibit a transition from a non-oscillating region to an oscillating region. However, the slope in the oscillating region differs for each Higgs vacua. Only the index for  $\square\square$  matches the large- $N$  entropy  $\tilde{S}$ , which clearly distinguishes the two indices. We therefore analyze the complex- $\beta$  phase diagrams of the two smooth Higgs vacuum indices individually to determine whether the phase diagrams also display different patterns for different Higgs vacua. The results are shown in Figures 13 and 14, respectively.

Most interestingly, the small peak observed in the phase diagram of the superconformal index appears only in that of the smooth index associated with  $\square\square + \square\square^T$ . The phase diagram for  $\square\square$  shows only a tiny bump, which is negligible compared to the other peaks. Although taking the unrefined limit causes us to lose detailed charge information about the states, the Young diagrams still hint at which charge sectors dominate at each Higgs

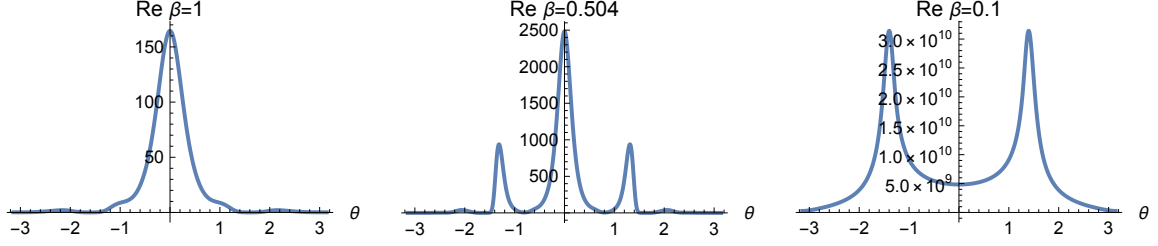


**Figure 13.** The complex- $\beta$  phase diagram of the smooth Higgs vacuum index for  $\square\square$ , evaluated at  $\text{Re } \beta = 1, 0.504, 0.1$ . The minor peak around  $\theta = \pm 2.04$  observed in the phase diagram of the complete superconformal index (Figure 6) does not appear here.

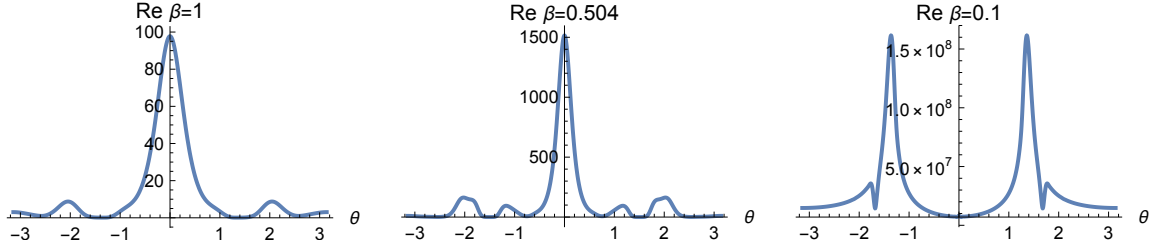


**Figure 14.** The complex- $\beta$  phase diagram of the smooth Higgs vacuum index for  $\square\square + \square\square^T$ , evaluated at  $\text{Re } \beta = 1, 0.504, 0.1$ . One can observe the same small peak around  $\theta = \pm 2.04$  that appears in the phase diagram of the complete superconformal index (Figure 6). However, for small  $\text{Re } \beta$ , eventually it is dominated by the peak around  $\theta = \pm 1.40$  corresponding to the known black hole contribution.

vacuum. For instance, comparing the Higgs vacuum indices in (3.1) and (3.3) associated with the linear Young diagrams, we find that (3.1) tends to have positive powers of  $z$ , corresponding to the excitation of the adjoint field  $Y$ , while (3.3) tends to have negative powers, corresponding to  $Z$ . It is thus natural to expect that a linear Young diagram captures states with biased charges, either  $Q_1 \gg Q_2$  or  $Q_1 \ll Q_2$  where  $Q_1$  and  $Q_2$ , two of the Cartans of  $\text{Spin}(8)_R$ , count roughly the excitations of the adjoint chirals  $Y$  and  $Z$ , respectively. This is in contrast to the standard black hole peak, which is expected to be dominated by states with approximately equal charges  $Q_1 \approx Q_2$ . Therefore, we need to investigate this charge sector to interpret the contribution of the small peak arising from Higgs vacua corresponding to the linear Young diagrams. A precise statement, however, requires the refined index with the complete charge information, which is beyond our current computational capabilities. It would be interesting to extend the refined computation to higher orders to better understand the nature of this small peak. In the next section, we will provide further evidence of this expectation using particular limits of the superconformal index, leading to the Hilbert series and the half-BPS indices of the ADHM quiver.

Another crucial observation is that even for the linear Young diagrams, the standard black hole peak dominates when  $\text{Re } \beta$  is small. See the right plot in Figure 14. Thus, we expect that although the slope of the index for  $\square\square + \square\square^T$  differs from that of the black hole entropy in the charge range up to  $Q = 100$ , the contribution from the standard black hole



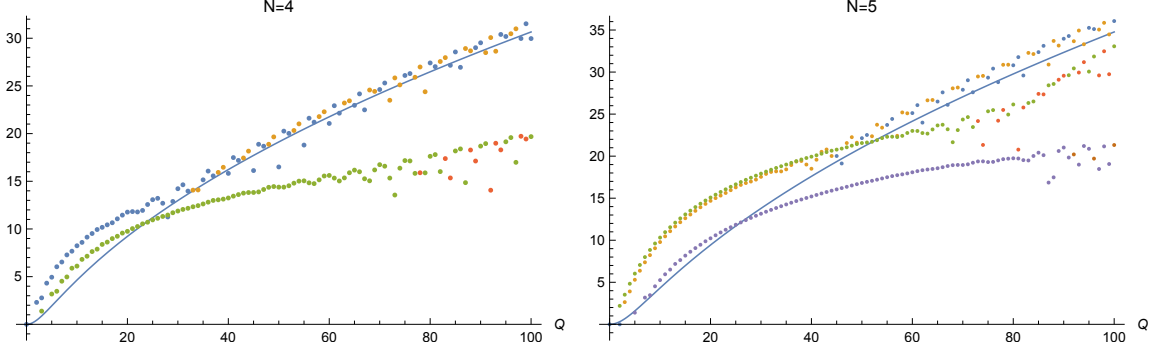


**Figure 15.** Two smooth Higgs vacuum indices for  $N = 4$  with vortex contributions up to vorticity 67 (left) and three for  $N = 5$  with vortex contributions up to vorticity 50 (right). For  $N = 4$ , the index corresponding to  $\square\square + \square\square + \square\square^T$  are represented by blue (positive sign) and orange (negative sign) dots, whereas the index corresponding to  $\square\square\square + \square\square\square^T$  are represented by green (positive sign) and red (negative sign) dots. For  $N = 5$ , the index corresponding to  $\square\square\square + \square\square\square + \square\square\square^T$  are represented by blue (positive sign) and orange (negative sign) dots; the index corresponding to  $\square\square\square\square + \square\square\square\square^T$  by green (positive sign) and red (negative sign) dots; and the index corresponding to  $\square\square\square\square\square + \square\square\square\square\square^T$  by purple (positive sign) and brown (negative sign) dots. In both cases, the large- $N$  entropy  $\tilde{S}$  is shown by the blue lines.

solution should dominate at larger  $Q$ . It would be interesting to extend the computation to higher orders to confirm this expectation. In addition, this suggests that the contribution of the small peak cannot be seen by merely tracing the leading term in the large- $N$  limit, which will be dominated by the standard black hole solutions. This is, in fact, consistent with the Cardy-limit computation in [8], where it was shown that, in the Cardy limit, the superconformal index reduces to the contribution of the linear Young diagrams. Therefore, to extract the information of the small peak, one should look at a restricted charge sector where the standard black hole contribution is suppressed.

The indices for  $N = 4, 5$  are, on the other hand, calculated using the truncated vortex contributions, which lose the fine details of the index. For this reason, we relegate the analysis of their complex- $\beta$  phase diagrams to future study and instead provide only comparisons of the overall growth of smooth Higgs vacuum indices, which show similar patterns to the  $N = 3$  case. See Figure 15.

#### 4 Factorization of the 3d ADHM index with multiple flavors

While we have so far discussed the ADHM quiver with a single flavor, one can also consider the theory with  $F$  flavors. This theory arises as a UV gauge theory of the 3d SCFT describing the low-energy dynamics of M2-branes probing the singularity  $\mathbb{C}^2 \times \mathbb{C}^2/\mathbb{Z}_F$  [56], whose holographic dual is M-theory on  $\text{AdS}_4 \times S^7/\mathbb{Z}_F$ . Famously, the Higgs branch of the ADHM quiver is the moduli space of  $N$  instantons for the  $U(F)$  gauge theory [33], while

its Coulomb branch is given by the symmetric product of  $N$  copies of the orbifold  $\mathbb{C}^2/\mathbb{Z}_F$ , i.e.,  $\text{Sym}^N(\mathbb{C}^2/\mathbb{Z}_F)$  [57], which is the same as the  $N$ -instanton moduli space when  $F = 1$ . The Higgs and Coulomb branches are no longer identical when  $F > 1$ , indicating that the theory is not self-mirror, unlike the single-flavor case. Instead, its mirror dual is a circular quiver of  $F$   $U(N)$  gauge nodes with one flavor attached to a single node, which is a special case of the Kronheimer–Nakajima quiver [58]. In addition, as evident from the geometry, the supersymmetry is not enhanced and remains as  $\mathcal{N} = 4$  in the IR if  $F > 1$ .

One can write down the index for the theory with multiple flavors, again using the matrix integral formula:

$$\begin{aligned} \mathcal{I}(w, z, t, q) = & \quad (4.1) \\ & \frac{1}{N!} \sum_{m \in \mathbb{Z}^N / S_N} \oint \left( \prod_{a=1}^N \frac{ds_a}{2\pi i s_a} w^{m_a} t^{-F|m_a|/2} q^{F|m_a|/2} \right) \times \\ & \left( \prod_{1 \leq a \neq b \leq N} \left( 1 - s_a s_b^{-1} q^{|m_a - m_b|} \right) \right) \left( \prod_{i=1}^F \prod_{a=1}^N \frac{(s_a^{-1} y_i t^{-\frac{1}{2}} q^{\frac{3}{2} + |m_a|}; q^2)}{(s_a y_i^{-1} t^{\frac{1}{2}} q^{\frac{1}{2} + |m_a|}; q^2)} \frac{(s_a y_i^{-1} t^{-\frac{1}{2}} q^{\frac{3}{2} + |m_a|}; q^2)}{(s_a^{-1} y_i t^{\frac{1}{2}} q^{\frac{1}{2} + |m_a|}; q^2)} \right) \times \\ & \left( \prod_{a,b=1}^N \frac{(s_a^{-1} s_b t q^{1+|-m_a+m_b|}; q^2) (s_a^{-1} s_b z^{-1} t^{-\frac{1}{2}} q^{\frac{3}{2}+|-m_a+m_b|}; q^2) (s_a^{-1} s_b z t^{-\frac{1}{2}} q^{\frac{3}{2}+|-m_a+m_b|}; q^2)}{(s_a s_b^{-1} t^{-1} q^{1+|m_a-m_b|}; q^2) (s_a s_b^{-1} z t^{\frac{1}{2}} q^{\frac{1}{2}+|m_a-m_b|}; q^2) (s_a s_b^{-1} z^{-1} t^{\frac{1}{2}} q^{\frac{1}{2}+|m_a-m_b|}; q^2)} \right) \end{aligned} \quad (4.2)$$

where we have again used the shorthand  $(a; q^2)$  for the q-Pochhammer symbol  $(a; q^2)_\infty = \prod_{k=0}^\infty (1 - a q^{2k})$ . On top of the symmetries of the single-flavor case shown in Table 1, now we also have the  $SU(F)$  flavor symmetry under which the flavors form the fundamental representation, whose fugacities  $y_i$  satisfy  $\prod_{i=1}^F y_i = 1$ .

This integral formula is useful to study the large- $N$  limit of the index. For instance, the large- $N$  free energy can be obtained using the Cardy block formalism [29]:

$$\mathcal{F} = -\log \mathcal{I} \approx i \frac{4\sqrt{2} F^{\frac{1}{2}} N^{\frac{3}{2}}}{3} \frac{\sqrt{\Delta_1 \Delta_2 \Delta_3 \Delta_4}}{2\beta}, \quad (4.3)$$

where we have an additional factor of  $F^{\frac{1}{2}}$  compared to that of the single-flavor theory. Note that there is no  $y_i$ -dependence in this leading contribution. Despite its usefulness in the large- $N$  analysis, however, the matrix integral formula is inefficient for computing finite- $N$  indices. Thus, our goal here is to derive an alternative formula using the factorization of the superconformal index for multiple flavors.

The derivation is almost identical to that of the single-flavor case; therefore, we explain it focusing on the differences. In (4.1), the integration contour for each  $s_a$  is taken as the unit circle. Then we can evaluate this integral by taking the residues at the poles outside the contour. Assuming  $|q| < 1$  and  $|t| = |z| = |y_i| = 1$ , the poles sitting outside the unit

circle are determined as the intersections of the following hyperplanes:

$$s_a = y_i t^{-\frac{1}{2}} q^{-\frac{1}{2}} q^{-|m_a|-2k_a}, \quad (4.4)$$

$$s_a = s_b z^{-1} t^{-\frac{1}{2}} q^{-\frac{1}{2}} q^{-|m_a-m_b|-2k_a}, \quad (4.5)$$

$$s_a = s_b z t^{-\frac{1}{2}} q^{-\frac{1}{2}} q^{-|m_a-m_b|-2k_a}, \quad (4.6)$$

$$s_a = s_b t q^{-1} q^{-|m_a-m_b|-2k_a} \quad (4.7)$$

with  $k_a \geq 0$ . As noted in [8], a pole intersecting the last type of hyperplanes has the vanishing residue, and the relevant poles are only those determined by the other three. Thus, the residue calculation is essentially the same as that of two-adjoint theories, whose poles are generically labeled by binary trees [42]. The root node represents the first-type hyperplane, and its two child nodes, as well as their descendants, correspond to the second and the third-type hyperplanes.

In [8], it was argued that for the 3d ADHM theory with a single flavor, the poles having nontrivial residues are only those whose corresponding binary tree can be mapped to a Young diagram. Under this mapping, the initial box of the Young diagram, located at position (1, 1), represents the root node of the binary tree, while each box that is vertically or horizontally adjacent to a previously assigned box corresponds to a child node of that node, defined recursively. This reflects the facts that the trees having no counterpart Young diagrams have vanishing residues, and that the would-be higher order poles are rendered simple by additional zeros arising from the superpotential constraints on the fugacities. The important point is that this argument only relates to how the second and the third-type hyperplanes intersect, and it is independent of the first-type hyperplane. Thus, as long as each  $y_i$  has a generic value so that no accidental pole or zero arises, it is still valid for multiple flavors, as the number of flavors only affects the first-type hyperplanes.

More precisely, for  $F$  flavors, we have  $F$  hyperplanes of the first type distinguished by  $y_i$ . Thus, the poles are now labeled by a set of  $F$  colored Young diagrams of  $N$  boxes in total. Other than this, the remaining calculation is the same as that of the single-flavor case, which in the end results in the following form of the index:

$$\mathcal{I}(\vec{y}, w, z, t, q) = \sum_{\sum_{i=1}^F |\mathcal{Y}_i| = N} Z_{\text{pert}}^{\vec{\mathcal{Y}}}(\vec{y}, z, t, q) Z_{\text{vort}}^{\vec{\mathcal{Y}}}(\vec{y}, w, z, t, q) Z_{\text{vort}}^{\vec{\mathcal{Y}}}(\vec{y}^{-1}, w^{-1}, z^{-1}, t^{-1}, q^{-1}) \quad (4.8)$$

with

$$\begin{aligned} Z_{\text{pert}}^{\vec{\mathcal{Y}}}(\vec{y}, z, t, q) = & \left( \prod_{\mathbf{a} \neq \mathbf{b} \in \vec{\mathcal{Y}}} (1 - v_{\mathbf{a}}^{-1} v_{\mathbf{b}}) \right) \left( \prod_{i=1}^F \prod_{\mathbf{a} \in \vec{\mathcal{Y}}} \frac{(v_{\mathbf{a}} y_i q^2; q^2)}{(v_{\mathbf{a}}^{-1} y_i^{-1}; q^2)} \frac{(v_{\mathbf{a}}^{-1} y_i^{-1} (tq)^{-1} q^2; q^2)}{(v_{\mathbf{a}} y_i tq; q^2)} \right) \\ & \times \left( \prod_{\mathbf{a}, \mathbf{b} \in \vec{\mathcal{Y}}} \frac{(v_{\mathbf{a}} v_{\mathbf{b}}^{-1} tq; q^2) (v_{\mathbf{a}} v_{\mathbf{b}}^{-1} (zt^{\frac{1}{2}} q^{\frac{1}{2}})^{-1} q^2; q^2) (v_{\mathbf{a}} v_{\mathbf{b}}^{-1} (z^{-1} t^{\frac{1}{2}} q^{\frac{1}{2}})^{-1} q^2; q^2)}{(v_{\mathbf{a}}^{-1} v_{\mathbf{b}} (tq)^{-1} q^2; q^2) (v_{\mathbf{a}}^{-1} v_{\mathbf{b}} z t^{\frac{1}{2}} q^{\frac{1}{2}}; q^2) (v_{\mathbf{a}}^{-1} v_{\mathbf{b}} z^{-1} t^{\frac{1}{2}} q^{\frac{1}{2}}; q^2)} \right), \end{aligned} \quad (4.9)$$

$$Z_{\text{vort}}^{\vec{\mathcal{Y}}}(\vec{y}, w, z, t, q) = \sum_{k_a} \left( wt^{\frac{F}{2}} q^{-\frac{F}{2}} \right)^{\sum_{a \in \vec{\mathcal{Y}}} k_a} \left( \prod_{i=1}^F \prod_{a \in \vec{\mathcal{Y}}} \frac{(v_a^{-1} y_i^{-1}; q^2)_{-k_a}}{(v_a^{-1} y_i^{-1} t^{-1} q; q^2)_{-k_a}} \right) \\ \times \left( \prod_{a \neq b \in \vec{\mathcal{Y}}} \frac{(v_a^{-1} v_b z t^{\frac{1}{2}} q^{\frac{1}{2}}; q^2)_{-k_a+k_b} (v_a^{-1} v_b t^{-1} q; q^2)_{-k_a+k_b}}{(v_a^{-1} v_b; q^2)_{-k_a+k_b} (v_a^{-1} v_b z t^{-\frac{1}{2}} q^{\frac{3}{2}}; q^2)_{-k_a+k_b}} \right) \quad (4.10)$$

where the vanishing factors appearing in the expression must be discarded. Here,  $v_a$  for  $a \in \mathcal{Y}_i$  is given by

$$v_a = y_i^{-1} z^{i(a)-j(a)} (tq)^{\frac{1}{2}(i(a)+j(a)-2)} \quad (4.11)$$

where  $(i(a), j(a))$  is the position of box  $a$  in Young diagram  $\mathcal{Y}_i$ .  $k_a$ , a combination of  $\vec{m}$  and  $\vec{k}$ , is a non-negative integer assigned to each  $a$  such that those integers are non-decreasing along each row and column of  $\mathcal{Y}_i$  starting from the initial box. See [8] for further details of the computations.

In the remainder of this section, we will give a brief discussion of examples and also examine a useful limit of this expression, which leads to a new formula for the refined Higgs branch Hilbert series, capturing BPS states annihilated by two complex supercharges.

#### 4.1 Examples

As an example, let us consider the  $U(2)$  ADHM with two flavors. With generic real masses, the theory has five discrete Higgs vacua labeled by the following colored Young diagrams:

$$\begin{array}{c} \blacksquare \\ \blacksquare \end{array} \oplus \begin{array}{cc} \blacksquare & \blacksquare \end{array} \oplus \begin{array}{c} \blacksquare \\ \blacksquare \end{array} \oplus \begin{array}{cc} \blacksquare & \blacksquare \end{array} \oplus \begin{array}{c} \blacksquare \\ \blacksquare \end{array} \oplus \begin{array}{cc} \blacksquare & \blacksquare \end{array} \quad (4.12)$$

where blue Young diagrams are associated with  $y_1 = y$ , while red Young diagrams correspond to  $y_2 = 1/y$ . The index evaluated at each vacuum is given by

$$\begin{array}{c} \blacksquare \\ \blacksquare \end{array} : \quad q^{\frac{1}{2}} \frac{y^{-3} z^2}{(y - y^{-1})(z - z^{-1})} + q \left[ -\frac{y^{-2} z}{z - z^{-1}} + \frac{y^{-4} z^3 (y + y^{-1})}{(y - y^{-1})(z - z^{-1})} \right] \\ + q^{3/2} \left[ -\frac{y^{-3} z^2 (y + y^{-1})}{z - z^{-1}} + \frac{y^{-7} z^4 + y^{-4} z^3 (y + y^{-1})(z + z^{-1})}{(y - y^{-1})(z - z^{-1})} \right. \\ \left. + \frac{y^{-2} z^2 (z + z^{-1})}{2} \left( \frac{y + y^{-1}}{y - y^{-1}} - \frac{z + z^{-1}}{z - z^{-1}} \right) \right] + \dots \quad (4.13)$$

$$\begin{array}{cc} \blacksquare & \blacksquare \end{array} : \quad (z \leftrightarrow z^{-1}) \quad (4.14)$$

$$\begin{array}{c} \blacksquare \\ \blacksquare \end{array} : \quad (y \leftrightarrow y^{-1}) \quad (4.15)$$

$$\begin{array}{cc} \blacksquare & \blacksquare \end{array} : \quad (y \leftrightarrow y^{-1} \ \& \ z \leftrightarrow z^{-1}) \quad (4.16)$$

$$\begin{array}{c} \blacksquare \quad \blacksquare \end{array} : \quad 1 + q^{\frac{1}{2}} (1 + \chi_3) (z + z^{-1}) + q [2 + 2\chi_3 + (4 + \chi_3 + \chi_5) (z^2 + 1 + z^{-2})] \\ + q^{\frac{3}{2}} [(4 + 4\chi_3 + 2\chi_5) (z + z^{-1}) + (2 + 2\chi_3 + \chi_5 + \chi_7) (z^3 + z + z^{-1} + z^{-3})] \\ + \dots \quad (4.17)$$

where one can use the permutation symmetries  $y \leftrightarrow y^{-1}$  and  $z \leftrightarrow z^{-1}$  to obtain other three indices from the first one. In the last line, we have used the  $SU(2)$  flavor character  $\chi_n = \sum_{k=-\frac{n-1}{2}}^{\frac{n-1}{2}} y^{2k}$  of dimension  $n$ . By summing these contributions, one obtains the complete superconformal index as follows:

$$I_{N=2;F=2}(\vec{y}, w, z, t, q) = 1 + q^{\frac{1}{2}} (z + z^{-1}) + q (3 + \chi_3 + 2 (z^2 + 1 + z^{-2})) \\ + q^{\frac{3}{2}} ((6 + 2\chi_3) (z + z^{-1}) + 2 (z^3 + z + z^{-1} + z^{-3})) + \dots \quad (4.18)$$

The indices for other values of  $N$  and  $F$  can also be obtained using the formula (4.8).

One may also attempt to compare finite- $N$  indices of multi-flavor cases with the result from the large- $N$  analysis. Recall that the large- $N$  limit of the index with multiple flavors is governed by free energy (4.3). Since the only difference is the additional factor of  $F^{\frac{1}{2}}$ , one can easily obtain the large- $N$  entropy as follows:

$$S_{N;F}(Q) = S(Q; F^{\frac{1}{2}} N^{\frac{3}{2}}) \quad (4.19)$$

where  $S$  on the right hand side is the entropy for a single flavor given in (2.15). Now we can compare  $S_{N;F}$  with the logarithm of the unrefined indices at finite  $N$  with multiple flavors, whose results are shown in Figure 16 for  $N = 1, 2, 3$  and  $F = 2$ . Again, we observe that the large- $N$  entropy provides a good approximation to the finite- $N$  indices. While a detailed examination of the complex- $\beta$  phase diagrams of these indices would also be of interest, we leave this to future work.

## 4.2 Limit to the Higgs branch Hilbert series

The Hilbert series is the observable that encodes the data of (a branch of) the moduli space of vacua as an algebraic variety. For 3d  $\mathcal{N} = 4$  theories, one can mainly consider two types of it: the Higgs branch Hilbert series and the Coulomb branch Hilbert series. In particular, for ‘good’  $\mathcal{N} = 4$  gauge theories in the sense of Gaiotto–Witten, these Hilbert series can be obtained as particular limits of the superconformal index [31].<sup>8</sup> In our case, the limits are given by

$$\text{Higgs branch limit : } q, t^{-1} \rightarrow 0, \quad qt \text{ fixed}, \quad (4.20)$$

$$\text{Coulomb branch limit : } q, t \rightarrow 0, \quad q/t \text{ fixed}. \quad (4.21)$$

Roughly speaking, the Higgs limit removes the contribution of monopole operators from the index while retaining that of the adjoint hypermultiplet, whereas the Coulomb limit removes the contribution of the adjoint hypermultiplet while retaining that of monopole operators. This is reflected to the BPS condition. Recall that the BPS condition for the states contributing the superconformal index satisfy

$$E = \frac{1}{2} (Q_1 + Q_2 + Q_3 + Q_4) + j, \quad (4.22)$$

---

<sup>8</sup>For 3d  $\mathcal{N} = 2$  theories, the distinction between the Higgs and Coulomb branches are not always clear. Nevertheless, one can obtain the Hilbert series of a certain ‘component’ of the moduli space by taking a suitable limit of the superconformal index [59].

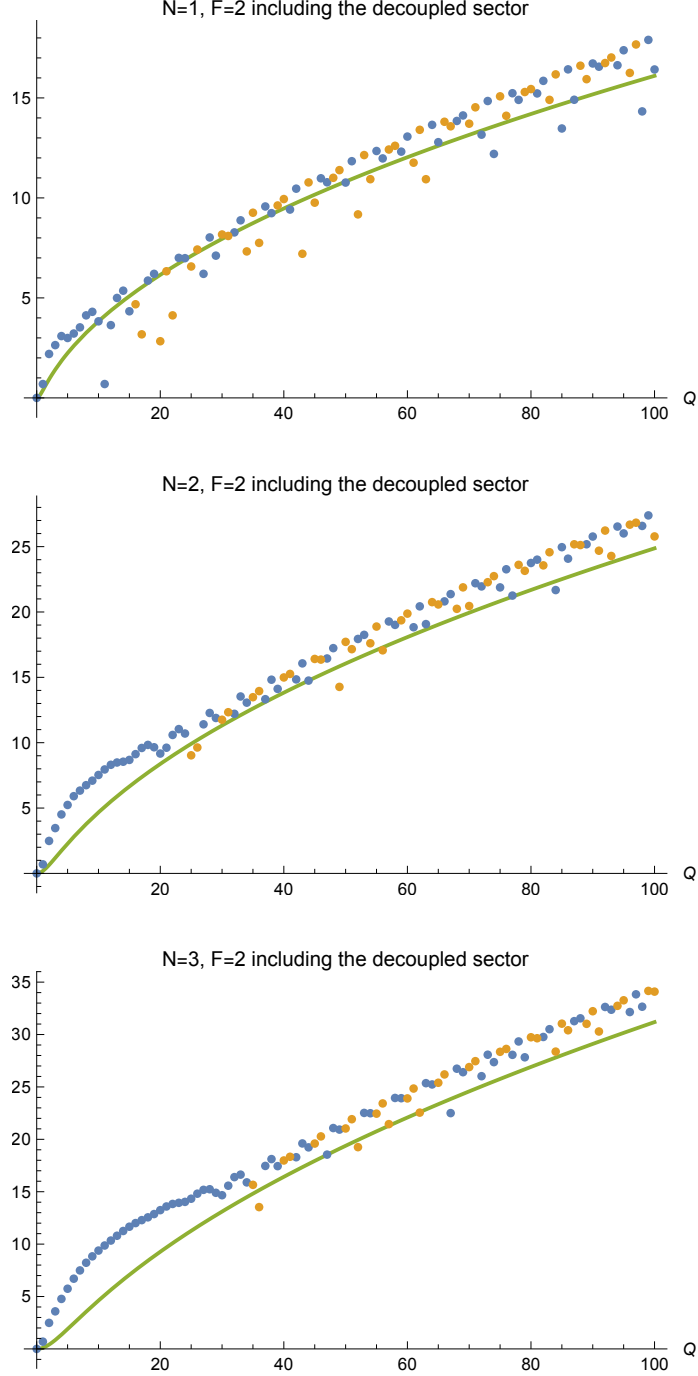


**Figure 16.**  $\log I_{N=1,2,3; F=2}(Q)$  (blue & orange dots) vs  $S_{N=1,2,3; F=2}(Q)$  (green line) up to  $x^{100}$ . Blue and orange dots represent coefficients with positive and negative signs, respectively. The agreement improves with increasing  $N$ .

where  $Q_i$ 's are integer-quantized Cartans of the  $Spin(8)_R$  symmetry. On the other hand, the states contributing to the Hilbert series are annihilated by two complex supercharges

and satisfy the following relation:

$$\text{Higgs branch limit : } E = \frac{1}{2}(Q_1 + Q_2), \quad Q_3 = Q_4 = j = 0, \quad (4.23)$$

$$\text{Coulomb branch limit : } E = \frac{1}{2}(Q_3 + Q_4), \quad Q_1 = Q_2 = j = 0. \quad (4.24)$$

Among these two limits, we focus on the Higgs branch limit, in which our factorized index naturally leads to a new and simple formula for the Higgs branch Hilbert series. First, it is straightforward to show that, in the  $w$ -expansion of  $Z_{\text{vort}}^{\vec{\mathcal{Y}}}$  in (2.9), each power of  $w$  is accompanied by at least a factor of  $q/t$ , which vanishes in the Higgs limit. Consequently,  $Z_{\text{vort}}^{\vec{\mathcal{Y}}}$  goes to 1, and we are left only with  $Z_{\text{pert}}^{\vec{\mathcal{Y}}}$ . In the same limit,  $Z_{\text{pert}}^{\vec{\mathcal{Y}}}$  becomes

$$\lim_{\substack{q, t^{-1} \rightarrow 0 \\ r \equiv (qt)^{\frac{1}{2}} \text{ fixed}}} Z_{\text{pert}}^{\vec{\mathcal{Y}}}(\vec{y}, z, q) \quad (4.25)$$

$$\begin{aligned} \rightarrow H^{\vec{\mathcal{Y}}}(\vec{y}, z, r) &= \left( \prod_{\mathbf{a} \neq \mathbf{b} \in \vec{\mathcal{Y}}} (1 - v_{\mathbf{a}}^{-1} v_{\mathbf{b}}) \right) \left( \prod_{i=1}^F \prod_{\mathbf{a} \in \vec{\mathcal{Y}}} \frac{1}{(1 - v_{\mathbf{a}}^{-1} y_i^{-1})} \frac{1}{(1 - v_{\mathbf{a}} y_i r^2)} \right) \\ &\quad \times \left( \prod_{\mathbf{a}, \mathbf{b} \in \vec{\mathcal{Y}}} \frac{(1 - v_{\mathbf{a}} v_{\mathbf{b}}^{-1} r^2)}{(1 - v_{\mathbf{a}}^{-1} v_{\mathbf{b}} z r)(1 - v_{\mathbf{a}}^{-1} v_{\mathbf{b}} z^{-1} r)} \right) \end{aligned} \quad (4.26)$$

where the vanishing factors must be discarded as in the case of the superconformal index.  $v_{\mathbf{a}}$  for  $\mathbf{a} \in \mathcal{Y}_i$  is now given by

$$v_{\mathbf{a}} = y_i^{-1} z^{i(\mathbf{a}) - j(\mathbf{a})} r^{i(\mathbf{a}) + j(\mathbf{a}) - 2} \quad (4.27)$$

where, as before,  $(i(\mathbf{a}), j(\mathbf{a}))$  is the position of the box  $\mathbf{a}$  in Young diagram  $\mathcal{Y}_i$ . As a result, the (refined) Higgs branch Hilbert series is given by the following simple formula:

$$\mathcal{H}_{N;F}(\vec{y}, z, r) = \sum_{\sum_{i=1}^F |\mathcal{Y}_i| = N} H^{\vec{\mathcal{Y}}}(\vec{y}, z, r). \quad (4.28)$$

For  $F = 1$ , the Higgs and Coulomb branches are identical since the theory is self-mirror. Thus, (4.28) also corresponds to the Coulomb branch Hilbert series of the ADHM with a single flavor, where  $z$  is now associated with the topological  $U(1)$  symmetry acting on monopole operators instead of the adjoint hyper.

In fact, the same formula for  $F = 1$  was obtained in [60]. Also, there are alternative expressions obtained from the Coulomb branch side [61, 62]. For instance, the following expression is obtained using the Fermi-gas method [61]:

$$\mathcal{H}_{N;F=1} \left( z = (x_1/x_2)^{\frac{1}{2}}, r = (x_1 x_2)^{\frac{1}{2}} \right) = \sum_{|\lambda|=N} \prod_{i=1}^r \frac{Z_{\lambda_i}[\mathbb{C}^4; N](x_1; x_2)^{m_i}}{\lambda_i^{m_i} m_i!} \quad (4.29)$$

where

$$Z_i[\mathbb{C}^4; N](x_1; x_2) = \frac{1}{(1 - x_1^i)(1 - x_2^i)}. \quad (4.30)$$

We have confirmed the equality of the two expressions for several values of  $N$ . Note that (4.29) also involves a Young diagram summation, but its interpretation differs from that in our formula: in our case, the Young diagrams are associated with discrete Higgs vacua, whereas in (4.29) they are related to counting of monopole fluxes. This distinction reflects the self-mirror symmetry of the theory, which exchanges the Higgs and Coulomb branches. Additionally, it was also checked that (4.29) can be re-expanded in terms of giant graviton contributions [63].

Moreover, one can take further limits of the Higgs branch Hilbert series:

$$r, z^{-1} \rightarrow 0, \quad rz \text{ fixed}, \quad (4.31)$$

$$r, z \rightarrow 0, \quad r/z \text{ fixed}, \quad (4.32)$$

leading to the indices for half-BPS states. In each limit, only the contribution from the linear Young diagram  $\square \cdots \square^T$  or  $\square \cdots \square$  survives, respectively; namely,

$$\lim_{\substack{r, z^{-1} \rightarrow 0 \\ s \equiv rz \text{ fixed}}} \mathcal{H}_{N; F=1} = \begin{cases} \prod_{i=1}^N \frac{1}{1-s^i}, & \text{for } \square \cdots \square^T, \\ 0, & \text{otherwise.} \end{cases} \quad (4.33)$$

$$\lim_{\substack{r, z \rightarrow 0 \\ s \equiv r/z \text{ fixed}}} \mathcal{H}_{N; F=1} = \begin{cases} \prod_{i=1}^N \frac{1}{1-s^i}, & \text{for } \square \cdots \square, \\ 0, & \text{otherwise,} \end{cases} \quad (4.34)$$

This is consistent with our expectation discussed in the previous section that the linear Young diagrams capture biased charge sectors,  $Q_1 \gg Q_2$  and  $Q_1 \ll Q_2$ , as the states contributing these half-BPS indices satisfy

$$E = Q_1, \quad Q_2 = Q_3 = Q_4 = j = 0, \quad (4.35)$$

$$E = Q_2, \quad Q_1 = Q_3 = Q_4 = j = 0, \quad (4.36)$$

respectively.

For multiple flavors, on the other hand, the theory is no longer self-mirror; instead its mirror dual is given by a circular quiver of  $F$   $U(N)$  gauge nodes one of which has a single flavor attached. Thus, (4.28) also corresponds to the Coulomb Hilbert series of the mirror circular quiver, where  $\vec{y}$  and  $z$  are now associated with FI parameters for the topological  $U(1)$  symmetries rather than flavor real masses. As far as we are aware, (4.28) has not been derived in the literature, although there are alternative expressions [60, 62], which involve the *infinite* summations over Young diagrams of arbitrary size. In contrast, our expression restricts the contributing Young diagrams to the fixed total size  $N$ , providing a closed-form answer without infinite summations for a given  $N$ . It would be interesting to understand the analytic relation among these expressions.



One can also take the half-BPS limit, in which, again, only the linear Young diagrams contribute to the index. For instance, if we consider the limit (4.31) for the  $N = F = 2$  case, the contributing Young diagrams are as follows:

$$\begin{array}{|c|} \hline \text{blue square} \\ \hline \end{array} : \frac{ry^{-4}}{(1-r)(1-r^2)(1-y^{-2})(1-ry^{-2})} \quad (4.37)$$

$$\begin{array}{|c|} \hline \text{red square} \\ \hline \end{array} : \frac{ry^4}{(1-r)(1-r^2)(1-y^2)(1-ry^2)} \quad (4.38)$$

$$\begin{array}{|c|c|} \hline \text{blue square} & \text{red square} \\ \hline \end{array} : \frac{1}{(1-r)^2(1-ry^{-2})(1-ry^2)} \quad (4.39)$$

The complete half-BPS index is given by

$$\mathcal{I}_{N=2;F=2}^{\text{half-BPS}}(s) = \frac{1}{(1-s)(1-s^2)}, \quad (4.40)$$

or generally,

$$\mathcal{I}_{N;F}^{\text{half-BPS}}(s) = \prod_{i=1}^N \frac{1}{1-s^i}, \quad (4.41)$$

which reproduces the result of [63]. We have confirmed this result for several values of  $N$  and  $F$ . Note that the result after the summation is independent of  $F$  and the flavor fugacities  $y_i$ .

## 5 Discussion

In this work, we have analyzed both the microcanonical and canonical aspects of the superconformal index for the 3d ADHM quiver gauge theory, which provides a UV description of the 3d  $\mathcal{N} = 8$  SCFT dual to M-theory on  $\text{AdS}_4 \times S^7$ . By computing the index to sufficiently high orders using the factorized index, we probed the finite- $N$  spectrum beyond the reach of the standard matrix integral formula. Our results reveal clear signatures of quantum black hole states: the finite- $N$  degeneracies of the ADHM quiver exhibit remarkable agreement with the leading large- $N$  contribution, which reproduces the holographic dual black hole entropy.

From the canonical perspective, we introduced the complex- $\beta$  phase diagram of the index, offering a new lens to visualize the contributions of distinct sets of states carrying different (complexified) entropies. This phase diagram exhibits multiple peaks, including subdominant structures that are suggestive of additional gravitational saddles beyond the standard graviton and black hole contributions.

We also discussed the generalization of the factorized index to the multi-flavor case, dual to M-theory on  $\text{AdS}_4 \times S^7/\mathbb{Z}_F$ , as well as its Higgs branch Hilbert series limit, which further illuminates the distribution of BPS states across discrete Higgs vacua, which remains invisible in the unrefined index.

Our study demonstrates that the finite- $N$  superconformal index is a powerful probe of the microscopic black hole states, and more broadly, of quantum-gravitational physics.

Nevertheless, several limitations remain. First, our analysis of the complex- $\beta$  phase diagram was carried out only for the  $N = 3$  case. For higher  $N$ , we have obtained phase diagrams with qualitatively similar multiple peaks, but these rely on approximate indices computed using truncated vortex contributions. While such truncation reliably captures the dominant contributions as explained in Section 2, it may not accurately resolve the finer, subdominant peaks. For this reason, we postpone a complete presentation of the higher- $N$  phase diagrams until more precise index data are available.

Second, our analysis focused on the unrefined index, which does not retain refined charge information of the states contributing to each peak in the phase diagram. Extending our study to the refined index is computationally challenging, but highly worthwhile, as it would provide sharper insight into the origin of the peaks and clarify their correspondence to distinct gravitational saddles.

Along these lines, it would be particularly interesting to investigate how the second peak at nonzero  $\theta$  observed in the  $N = 3$  case evolves for higher  $N$ , especially when refined charge information is included. In the unrefined index studied here, this peak remains subdominant for all values of  $\text{Re}\beta$ , which is the only (real) chemical potential available to tune. By contrast, the refined index introduces additional chemical potentials, making it natural to ask whether there exists a charge sector in which this subdominant peak could become dominant. Finally, it would be also interesting to analyze the indices of other models, such as 4d  $\mathcal{N} = 4$  SYM, using their complex- $\beta$  phase diagrams.

## Acknowledgments

We would like to thank Sung-Soo Kim and Kimyeong Lee for useful discussions. This work is supported by the National Natural Science Foundation of China under Grant No. 12247103.

## A Numerical index data

### A.1 $F = 1$

$Q$	$I(Q)$	$Q$	$I(Q)$	$Q$	$I(Q)$	$Q$	$I(Q)$
1	4	26	508	51	-14440	76	-43579
2	10	27	592	52	-1055	77	-249000
3	16	28	-212	53	18412	78	-5922
4	19	29	-664	54	7024	79	302512
5	20	30	264	55	-20864	80	79221
6	26	31	1288	56	-14355	81	-348812
7	40	32	491	57	22808	82	-177254
8	49	33	-1196	58	25120	83	382864
9	40	34	-794	59	-20952	84	304431
10	26	35	1592	60	-36570	85	-392332
11	40	36	1940	61	16820	86	-456322
12	84	37	-1064	62	50774	87	371544
13	100	38	-2614	63	-6872	88	634735
14	52	39	784	64	-64685	89	-305904
15	8	40	4038	65	-8136	90	-832436
16	64	41	772	66	78812	91	184840
17	172	42	-4510	67	31512	92	1042745
18	150	43	-2072	68	-88482	93	7284
19	-16	44	5503	69	-60984	94	-1248186
20	-61	45	4800	70	94128	95	-276960
21	172	46	-5158	71	99448	96	1436485
22	376	47	-7328	72	-90291	97	638384
23	152	48	4771	73	-144160	98	-1582312
24	-235	49	11284	74	75678	99	-1096384
25	-96	50	-2126	75	196072	100	1659947

**Table 2.**  $I_{N=1}(Q)$ .

$Q$	$I(Q)$	$Q$	$I(Q)$	$Q$	$I(Q)$	$Q$	$I(Q)$
1	4	26	53512	51	-3039696	76	253569860
2	20	27	35192	52	-5774712	77	436570264
3	56	28	7529	53	2096984	78	-173515228
4	139	29	27116	54	10016312	79	-662909992
5	260	30	95420	55	2420056	80	-18800137
6	436	31	118456	56	-12720055	81	897555608
7	640	32	31737	57	-8899188	82	370978500
8	954	33	-51484	58	14801988	83	-1075169544
9	1420	34	47252	59	20406648	84	-905873624
10	2076	35	255504	60	-10987758	85	1117450928
11	2720	36	241333	61	-33345668	86	1641225992
12	3234	37	-82896	62	1342452	87	-898257984
13	3780	38	-239576	63	48773112	88	-2536798887
14	5012	39	191560	64	20743090	89	285315372
15	7048	40	702809	65	-58643244	90	3510893952
16	8969	41	344652	66	-53725940	91	883764784
17	9372	42	-630708	67	60119072	92	-4379393839
18	9160	43	-608536	68	102064545	93	-2734051912
19	11504	44	915744	69	-39414584	94	4881456348
20	17743	45	1736912	70	-157547640	95	5359732192
21	22788	46	-102540	71	-9736832	96	-4622751190
22	20236	47	-2297376	72	215741446	97	-8722854996
23	14096	48	-669835	73	103428652	98	3130376152
24	19366	49	3480996	74	-254224568	99	12637829184
25	40104	50	3218668	75	-243562936	100	168588591

**Table 3.**  $I_{N=2}(Q)$ .

$Q$	$I(Q)$	$Q$	$I(Q)$	$Q$	$I(Q)$	$Q$	$I(Q)$
1	4	26	1686030	51	-159286180	76	-62074824537
2	20	27	1909628	52	-308279461	77	76102730060
3	76	28	2638781	53	165220072	78	136344817966
4	239	29	3730916	54	741621172	79	-40980922696
5	644	30	4313620	55	358313432	80	-226940640423
6	1512	31	3862944	56	-826171406	81	-57666714244
7	3100	32	3597751	57	-959372832	82	311772645310
8	5743	33	5632696	58	895231242	83	250591469676
9	9856	34	9545336	59	2313071704	84	-335087722422
10	16182	35	11012600	60	237084373	85	-545477313496
11	25988	36	7141251	61	-3323858932	86	220959177358
12	40764	37	3509216	62	-2192044918	87	924071216868
13	61252	38	10072680	63	4205208120	88	140650293476
14	87066	39	24834016	64	6328259945	89	-1294542646004
15	118372	40	28225032	65	-2497800124	90	-850960563252
16	159560	41	8349524	66	-11107330518	91	1486961159404
17	219668	42	-9181610	67	-2303809220	92	1983734619134
18	304214	43	16446364	68	16404416584	93	-1209489319964
19	404012	44	71198813	69	13586908084	94	-3488673536444
20	501321	45	73190244	70	-17158447216	95	85767262344
21	601724	46	-13749410	71	-30379175116	96	5129595055044
22	757308	47	-74428808	72	9750606932	97	2321893736312
23	1021096	48	36543082	73	52843060108	98	-6347858136498
24	1347744	49	225910956	74	15219775806	99	-6351325819584
25	1586892	50	180681696	75	-71782352304	100	6216576038392

**Table 4.**  $I_{N=3}(Q)$ .

$Q$	$I(Q)$	$Q$	$I(Q)$	$Q$	$I(Q)$	$Q$	$I(Q)$
1	4	26	36457560	51	-2436265004	76	(-6223609696918)
2	20	27	48853180	52	881969440	77	(440150937208)
3	76	28	62836622	53	13697547476	78	(10770560439192)
4	274	29	76771608	54	19817672520	79	(6747229719880)
5	844	30	92954408	55	3014230384	80	(-13060343807655)
6	2392	31	118862728	56	-20636056503	81	(-19683510863092)
7	6040	32	159603602	57	-8209785248	82	(8526603268424)
8	13973	33	206382512	58	46366358632	83	(38051178045278)
9	29456	34	240071416	59	70563025880	84	(11266819067398)
10	57756	35	259924364	60	-4803998984	85	(-54345275551784)
11	106244	36	307535466	61	-105051587688	86	(-53166253002008)
12	187074	37	431664844	62	-48141869368	87	(54116553589374)
13	318496	38	600954848	63	175601554672	88	(120668995097068)
14	528272	39	685943784	64	252380923892	89	(-10369840695414)
15	850008	40	620664946	65	-75030764316	90	(-200009550126532)
16	1320718	41	602804664	66	-452431986000	91	(-108042462665298)
17	1978348	42	965846444	67	-165080317008	92	(253014357573104)
18	2883596	43	1650608792	68	(704404668000)	93	(328870601862792)
19	4148536	44	1948412418	69	(858567144108)	94	(-200357949547956)
20	5949400	45	1302263040	70	(-509962889032)	95	(-643520918943108)
21	8453160	46	568794608	71	(-1759273627320)	96	(-71896254788310)
22	11716184	47	1628052208	72	(-326303271871)	97	(973940843911658)
23	15697320	48	4575915690	73	(2819208970726)	98	(696522596278186)
24	20578417	49	5925821840	74	(2636463393252)	99	(-1116983116530986)
25	27124976	50	2374288436	75	(-2772404318490)	100	(-1752536951200026)

**Table 5.**  $I_{N=4}(Q)$  obtained by keeping vortex contributions up to vorticity 67. The values for  $Q \leq 67$  are exact, whereas those for  $Q > 67$  are computed approximately due to truncated vortex contributions.

$Q$	$I(Q)$	$Q$	$I(Q)$	$Q$	$I(Q)$	$Q$	$I(Q)$
1	4	26	350266614	51	(113358021050)	76	(−170645601418566)
2	20	27	483346216	52	(225451238050)	77	(−694265104756)
3	76	28	663109157	53	(310570543402)	78	(315640337778406)
4	274	29	911336272	54	(231049497994)	79	(272683959004882)
5	900	30	1247902572	55	(45168594768)	80	(−328246800113430)
6	2742	31	1677024564	56	(89793256744)	81	(−740290896259610)
7	7720	32	2191866317	57	(589854003244)	82	(−2408722459444)
8	20218	33	2815773580	58	(1103040590064)	83	(1324774027470558)
9	49236	34	3649448462	59	(750528055608)	84	(1080373189587376)
10	112018	35	4838036988	60	(−456061230074)	85	(−1457715507653672)
11	238924	36	6417691493	61	(−786755064470)	86	(−3028964475617002)
12	481019	37	8193585416	62	(1394460860872)	87	(205167642457532)
13	920992	38	9940767856	63	(4294700538546)	88	(5485039399759195)
14	1692246	39	11942144420	64	(3083764505338)	89	(3909870278320838)
15	3007540	40	15207255260	65	(−3291613780886)	90	(−6523005137450692)
16	5198335	41	20530721688	66	(−6585369988742)	91	(−11736890493314968)
17	8752344	42	26862112292	67	(2730927754156)	92	(2450463341163749)
18	14340048	43	31447146968	68	(17686898075237)	93	(22162517646188370)
19	22837992	44	33588894373	69	(14103455632828)	94	(12371897841071696)
20	35414847	45	38728314996	70	(−16425609972754)	95	(−28840217071078398)
21	53759388	46	54987723746	71	(−36166437364526)	96	(−42416672830433973)
22	80431652	47	80471364948	72	(3447458674412)	97	(18105147531830566)
23	119056196	48	96426330751	73	(74601219250310)	98	(85406423169118680)
24	173985404	49	86624550748	74	(63873446706520)	99	(31653130184236946)
25	249562588	50	72964896878	75	(−74230558747910)	100	(−121177080926622458)

**Table 6.**  $I_{N=5}(Q)$  obtained by keeping vortex contributions up to vorticity 50. The values for  $Q \leq 50$  are exact, whereas those for  $Q > 50$  are computed approximately due to truncated vortex contributions.

## A.2 $F = 2$

$Q$	$I(Q)$	$Q$	$I(Q)$	$Q$	$I(Q)$	$Q$	$I(Q)$
1	2	26	-1667	51	138078	76	-1338068
2	9	27	494	52	-9664	77	4131852
3	14	28	3051	53	-187646	78	2963096
4	22	29	1228	54	-56129	79	-4390550
5	20	30	-3537	55	230122	80	-5085734
6	25	31	-3284	56	158687	81	4093812
7	34	32	3927	57	-247648	82	7674449
8	62	33	7182	58	-298296	83	-2966220
9	74	34	-1517	59	222776	84	-10603382
10	46	35	-10500	60	472972	85	709088
11	2	36	-2324	61	-128144	86	13631274
12	38	37	14354	62	-663423	87	2980470
13	148	38	10279	63	-56104	88	-16368176
14	213	39	-15090	64	850307	89	-8348734
15	76	40	-20788	65	357528	90	18294046
16	-108	41	12306	66	-991498	91	15573790
17	-24	42	34968	67	-790238	92	-18708245
18	353	43	-1348	68	1033051	93	-24674408
19	494	44	-47820	69	1360464	94	16746813
20	-17	45	-17358	70	-900663	95	35440914
21	-562	46	58752	71	-2044600	96	-11413509
22	-62	47	48122	72	520535	97	-47342460
23	1098	48	-60190	73	2800420	98	1665717
24	1082	49	-88378	74	198685	99	59485744
25	-714	50	47435	75	-3539082	100	13558479

**Table 7.**  $I_{N=1; F=2}(Q)$ .



$Q$	$I(Q)$	$Q$	$I(Q)$	$Q$	$I(Q)$	$Q$	$I(Q)$
1	2	26	-15266	51	-28214160	76	12730004128
2	12	27	89760	52	61644066	77	1700777478
3	32	28	214210	53	84398696	78	-17865168076
4	91	29	146002	54	-44252956	79	-11318144748
5	188	30	-127564	55	-159090032	80	20596465611
6	368	31	-226788	56	-25833842	81	26555242838
7	564	32	200596	57	234626916	82	-17167902542
8	854	33	755096	58	180963038	83	-46832954924
9	1208	34	471302	59	-256616892	84	2596389689
10	1864	35	-715756	60	-427916668	85	69017948570
11	2844	36	-1141120	61	150876730	86	28673929778
12	4058	37	614030	62	745701122	87	-86101815120
13	4838	38	2728480	63	192031300	88	-81132917251
14	5140	39	1350944	64	-1029986660	89	86284866690
15	5900	40	-3239544	65	-862244208	90	155704165064
16	9171	41	-4241858	66	1091715572	91	-52688258488
17	14714	42	2791982	67	1902555920	92	-246034118886
18	18594	43	9508748	68	-617476497	93	-35212471212
19	15524	44	2547134	69	-3191678700	94	334252481692
20	9598	45	-13354066	70	-765525846	95	197951788116
21	14984	46	-12706930	71	4376648244	96	-386636616504
22	39832	47	13840208	72	3430829013	97	-449083501630
23	62304	48	30513476	73	-4736102218	98	350962381742
24	44434	49	-1573688	74	-7524928328	99	784818996808
25	-8384	50	-49287570	75	3182379332	100	-157103700994

**Table 8.**  $I_{N=2; F=2}(Q)$ .

$Q$	$I(Q)$	$Q$	$I(Q)$	$Q$	$I(Q)$	$Q$	$I(Q)$
1	2	26	2708084	51	-3308754064	76	-2699508634343
2	12	27	3907564	52	-230049973	77	1537639946784
3	36	28	4140077	53	6029530202	78	5512050125397
4	118	29	2948354	54	5845459260	79	1215746735238
5	312	30	2341876	55	-5618994068	80	-8226198086744
6	813	31	5802064	56	-14913791837	81	-7491811260068
7	1790	32	13160275	57	-2066770584	82	8454529631001
8	3719	33	16702212	58	25138228634	83	17770846319294
9	6848	34	7968996	59	24520466528	84	-2092892125779
10	11892	35	-6294156	60	-24057200450	85	-30128441163626
11	19284	36	-752625	61	-61695234172	86	-16051554628012
12	30946	37	38298200	62	-6198559148	87	38248437191214
13	48948	38	73548473	63	102980876558	88	50120716717677
14	77036	39	37556394	64	91065106796	89	-29628592287948
15	115898	40	-64433556	65	-107147935712	90	-98709223017124
16	163979	41	-91665848	66	-237096548172	91	-14265605578870
17	217240	42	87814356	67	5916314192	92	148211427764085
18	283604	43	327519828	68	409752248143	93	113806793903852
19	387832	44	225162299	69	293533792096	94	-165141902737509
20	563242	45	-323563792	70	-478186311146	95	-280065359191784
21	799184	46	-640582725	71	-841397886796	96	91352261495653
22	1017841	47	112655698	72	200480758151	97	495272146154922
23	1133038	48	1422324777	73	1555322957980	98	151741714454716
24	1239764	49	1228364628	74	766396517490	99	-685731332901192
25	1675748	50	-1366691242	75	-2052489446980	100	-640733064860587

**Table 9.**  $I_{N=3; F=2}(Q)$ .

## References

- [1] C. Romelsberger, *Counting chiral primaries in  $N = 1$ ,  $d=4$  superconformal field theories*, *Nucl. Phys. B* **747** (2006) 329–353, [[hep-th/0510060](#)].
- [2] J. Kinney, J. M. Maldacena, S. Minwalla and S. Raju, *An Index for 4 dimensional super conformal theories*, *Commun. Math. Phys.* **275** (2007) 209–254, [[hep-th/0510251](#)].
- [3] J. Bhattacharya, S. Bhattacharyya, S. Minwalla and S. Raju, *Indices for Superconformal Field Theories in 3,5 and 6 Dimensions*, *JHEP* **02** (2008) 064, [[0801.1435](#)].
- [4] A. Cabo-Bizet, D. Cassani, D. Martelli and S. Murthy, *Microscopic origin of the Bekenstein-Hawking entropy of supersymmetric  $AdS_5$  black holes*, *JHEP* **10** (2019) 062, [[1810.11442](#)].
- [5] S. Choi, J. Kim, S. Kim and J. Nahmgoong, *Large  $AdS$  black holes from QFT*, [1810.12067](#).
- [6] F. Benini and E. Milan, *A Bethe Ansatz type formula for the superconformal index*, *Commun. Math. Phys.* **376** (2020) 1413–1440, [[1811.04107](#)].
- [7] S. Choi and S. Kim, *Large  $AdS_6$  black holes from  $CFT_5$* , *JHEP* **08** (2024) 228, [[1904.01164](#)].
- [8] S. Choi, C. Hwang and S. Kim, *Quantum vortices, M2-branes and black holes*, *JHEP* **09** (2024) 096, [[1908.02470](#)].
- [9] A. Zaffaroni,  *$AdS$  black holes, holography and localization*, *Living Rev. Rel.* **23** (2020) 2, [[1902.07176](#)].
- [10] F. Benini, K. Hristov and A. Zaffaroni, *Black hole microstates in  $AdS_4$  from supersymmetric localization*, *JHEP* **05** (2016) 054, [[1511.04085](#)].
- [11] S. Murthy, *Growth of the  $\frac{1}{16}$ -BPS index in 4d  $N = 4$  supersymmetric Yang-Mills theory*, *Phys. Rev. D* **105** (2022) L021903, [[2005.10843](#)].
- [12] P. Agarwal, S. Choi, J. Kim, S. Kim and J. Nahmgoong,  *$AdS$  black holes and finite  $N$  indices*, *Phys. Rev. D* **103** (2021) 126006, [[2005.11240](#)].
- [13] C.-M. Chang and Y.-H. Lin, *Holographic covering and the fortuity of black holes*, [2402.10129](#).
- [14] C.-M. Chang and Y.-H. Lin, *Words to describe a black hole*, *JHEP* **02** (2023) 109, [[2209.06728](#)].
- [15] S. Choi, S. Kim, E. Lee and J. Park, *The shape of non-graviton operators for  $SU(2)$* , *JHEP* **09** (2024) 029, [[2209.12696](#)].
- [16] S. Choi, S. Kim, E. Lee, S. Lee and J. Park, *Towards quantum black hole microstates*, *JHEP* **11** (2023) 175, [[2304.10155](#)].
- [17] J. Choi, S. Choi, S. Kim, J. Lee and S. Lee, *Finite  $N$  black hole cohomologies*, *JHEP* **12** (2024) 029, [[2312.16443](#)].
- [18] R. de Mello Koch, M. Kim, S. Kim, J. Lee and S. Lee, *Brane-fused black hole operators*, [2412.08695](#).
- [19] A. Gadde, E. Lee, R. Raj and S. Tomar, *Probing Non-Graviton Spectra in  $\mathcal{N} = 4$  SYM via BMN truncation and S-Duality*, [2506.13887](#).
- [20] S. Kim, *The Complete superconformal index for  $N=6$  Chern-Simons theory*, *Nucl. Phys. B* **821** (2009) 241–284, [[0903.4172](#)].

- [21] Y. Imamura and S. Yokoyama, *Index for three dimensional superconformal field theories with general R-charge assignments*, *JHEP* **04** (2011) 007, [[1101.0557](#)].
- [22] S. Pasquetti, *Factorisation of  $N = 2$  Theories on the Squashed 3-Sphere*, *JHEP* **04** (2012) 120, [[1111.6905](#)].
- [23] C. Beem, T. Dimofte and S. Pasquetti, *Holomorphic Blocks in Three Dimensions*, *JHEP* **12** (2014) 177, [[1211.1986](#)].
- [24] C. Hwang, H.-C. Kim and J. Park, *Factorization of the 3d superconformal index*, *JHEP* **08** (2014) 018, [[1211.6023](#)].
- [25] M. Taki, *Holomorphic Blocks for 3d Non-abelian Partition Functions*, [[1303.5915](#)].
- [26] M. Fujitsuka, M. Honda and Y. Yoshida, *Higgs branch localization of 3d  $\mathcal{N} = 2$  theories*, *PTEP* **2014** (2014) 123B02, [[1312.3627](#)].
- [27] F. Benini and W. Peelaers, *Higgs branch localization in three dimensions*, *JHEP* **05** (2014) 030, [[1312.6078](#)].
- [28] F. Benini and A. Zaffaroni, *A topologically twisted index for three-dimensional supersymmetric theories*, *JHEP* **07** (2015) 127, [[1504.03698](#)].
- [29] S. Choi and C. Hwang, *Universal 3d Cardy Block and Black Hole Entropy*, *JHEP* **03** (2020) 068, [[1911.01448](#)].
- [30] E. Colombo, S. M. Hosseini, D. Martelli, A. Pittelli and A. Zaffaroni, *Microstates of Accelerating and Supersymmetric  $AdS_4$  Black Holes from the Spindle Index*, *Phys. Rev. Lett.* **133** (2024) 031603, [[2404.07173](#)].
- [31] S. S. Razamat and B. Willett, *Down the rabbit hole with theories of class  $\mathcal{S}$* , *JHEP* **10** (2014) 099, [[1403.6107](#)].
- [32] O. Aharony, O. Bergman, D. L. Jafferis and J. Maldacena,  *$N=6$  superconformal Chern-Simons-matter theories, M2-branes and their gravity duals*, *JHEP* **10** (2008) 091, [[0806.1218](#)].
- [33] M. F. Atiyah, N. J. Hitchin, V. G. Drinfeld and Y. I. Manin, *Construction of Instantons*, *Phys. Lett. A* **65** (1978) 185–187.
- [34] S. M. Hosseini and N. Mekareeya, *Large  $N$  topologically twisted index: necklace quivers, dualities, and Sasaki-Einstein spaces*, *JHEP* **08** (2016) 089, [[1604.03397](#)].
- [35] S. M. Hosseini and A. Zaffaroni, *The large  $N$  limit of topologically twisted indices: a direct approach*, *JHEP* **12** (2022) 025, [[2209.09274](#)].
- [36] J. Nian and L. A. Pando Zayas, *Microscopic entropy of rotating electrically charged  $AdS_4$  black holes from field theory localization*, *JHEP* **03** (2020) 081, [[1909.07943](#)].
- [37] O. Aharony, F. Benini, O. Mamroud and E. Milan, *A gravity interpretation for the Bethe Ansatz expansion of the  $\mathcal{N} = 4$  SYM index*, *Phys. Rev. D* **104** (2021) 086026, [[2104.13932](#)].
- [38] S. Choi, S. Jeong, S. Kim and E. Lee, *Exact QFT duals of  $AdS$  black holes*, *JHEP* **09** (2023) 138, [[2111.10720](#)].
- [39] S. Choi, D. Jain, S. Kim, V. Krishna, G. Kwon, E. Lee et al., *Supersymmetric Grey Galaxies, Dual Dressed Black Holes and the Superconformal Index*, [[2501.17217](#)].
- [40] E. Deddo, L. A. Pando Zayas and W. Zhou, *The superconformal index and black hole instabilities*, *JHEP* **05** (2025) 170, [[2502.01614](#)].

- [41] C. Hwang and J. Park, *Factorization of the 3d superconformal index with an adjoint matter*, *JHEP* **11** (2015) 028, [[1506.03951](#)].
- [42] C. Hwang, H. Kim and J. Park, *On 3d Seiberg-Like Dualities with Two Adjoints*, *Fortsch. Phys.* **66** (2018) 1800064, [[1807.06198](#)].
- [43] S. Choi, C. Hwang, S. Kim and J. Nahmgoong, *Entropy Functions of BPS Black Holes in  $AdS_4$  and  $AdS_6$* , *J. Korean Phys. Soc.* **76** (2020) 101–108, [[1811.02158](#)].
- [44] K. A. Intriligator and N. Seiberg, *Mirror symmetry in three-dimensional gauge theories*, *Phys. Lett. B* **387** (1996) 513–519, [[hep-th/9607207](#)].
- [45] O. Aharony, *IR duality in  $d = 3$   $N=2$  supersymmetric  $USp(2N(c))$  and  $U(N(c))$  gauge theories*, *Phys. Lett. B* **404** (1997) 71–76, [[hep-th/9703215](#)].
- [46] L. E. Bottini, C. Hwang, S. Pasquetti and M. Sacchi, *4d S-duality wall and  $SL(2, \mathbb{Z})$  relations*, *JHEP* **03** (2022) 035, [[2110.08001](#)].
- [47] C. Hwang, S. Pasquetti and M. Sacchi, *Rethinking mirror symmetry as a local duality on fields*, *Phys. Rev. D* **106** (2022) 105014, [[2110.11362](#)].
- [48] R. Comi, C. Hwang, F. Marino, S. Pasquetti and M. Sacchi, *The  $SL(2, \mathbb{Z})$  dualization algorithm at work*, *JHEP* **06** (2023) 119, [[2212.10571](#)].
- [49] C. Krattenthaler, V. P. Spiridonov and G. S. Vartanov, *Superconformal indices of three-dimensional theories related by mirror symmetry*, *JHEP* **06** (2011) 008, [[1103.4075](#)].
- [50] C. Hwang, P. Yi and Y. Yoshida, *Fundamental Vortices, Wall-Crossing, and Particle-Vortex Duality*, *JHEP* **05** (2017) 099, [[1703.00213](#)].
- [51] S. Minwalla, *Restrictions imposed by superconformal invariance on quantum field theories*, *Adv. Theor. Math. Phys.* **2** (1998) 783–851, [[hep-th/9712074](#)].
- [52] J. McGreevy, L. Susskind and N. Toumbas, *Invasion of the giant gravitons from Anti-de Sitter space*, *JHEP* **06** (2000) 008, [[hep-th/0003075](#)].
- [53] D. Gaiotto and J. H. Lee, *The giant graviton expansion*, *JHEP* **08** (2024) 025, [[2109.02545](#)].
- [54] V. A. Kostelecky and M. J. Perry, *Solitonic black holes in gauged  $N=2$  supergravity*, *Phys. Lett. B* **371** (1996) 191–198, [[hep-th/9512222](#)].
- [55] O. Aharony, O. Mamroud, S. Nowik and M. Weissman, *Bethe Ansatz for the superconformal index with unequal angular momenta*, *Phys. Rev. D* **109** (2024) 085015, [[2402.03977](#)].
- [56] M. Porrati and A. Zaffaroni, *M theory origin of mirror symmetry in three-dimensional gauge theories*, *Nucl. Phys. B* **490** (1997) 107–120, [[hep-th/9611201](#)].
- [57] J. de Boer, K. Hori, H. Ooguri and Y. Oz, *Mirror symmetry in three-dimensional gauge theories, quivers and D-branes*, *Nucl. Phys. B* **493** (1997) 101–147, [[hep-th/9611063](#)].
- [58] P. B. Kronheimer and H. Nakajima, *Yang-Mills instantons on ALE gravitational instantons*, *Math. Ann.* **288** (1990) 263–307.
- [59] A. Hanany, C. Hwang, H. Kim, J. Park and R.-K. Seong, *Hilbert Series for Theories with Aharony Duals*, *JHEP* **11** (2015) 132, [[1505.02160](#)].
- [60] S. Crew, N. Dorey and D. Zhang, *Blocks and Vortices in the 3d ADHM Quiver Gauge Theory*, *JHEP* **03** (2021) 234, [[2010.09732](#)].
- [61] H. Hayashi, T. Nosaka and T. Okazaki, *Dualities and flavored indices of M2-brane SCFTs*, *JHEP* **10** (2022) 023, [[2206.05362](#)].

- [62] H. Hayashi, T. Nosaka and T. Okazaki, *ADHM wilson line defect indices*, *JHEP* **09** (2024) [123](#), [[2406.00413](#)].
- [63] H. Hayashi, T. Nosaka and T. Okazaki, *M2-M5 giant graviton expansions*, *JHEP* **12** (2024) [109](#), [[2409.13239](#)].